POLITECNICO
MILANO 1863

SCUOLA DI INGEGNERIA INDUSTRIALE
E DELL'INFORMAZIONE

# Exploring the Idea of Dynamic Scaling using Froude Scaling Technique

Tesi di Laurea Magistrale in
Aeronautical Engineering - Ingegneria Aeronautica

Author: **Abdulmalek Salem A Shefat**

Student ID: 10715379
Advisor: Prof. Marco Lovera
Academic Year: 2021-22

# Abstract

Nowadays, the interest in Multirotor Unmanned Aerial Vehicles (UAVs) has increased exponentially[5] in various military and civil applications; these activities call for high-level requirements to be fulfilled by the design of high-performance and robust control laws, which usually relies on physical modeling of the system: system identification, which is the science of building mathematical models of dynamical processes from experimental data, play a significant role. Model identification tools are broadly available nowadays. The topic is mature enough to identify models with great certainty. However, the process is nowhere close to being accessible and requires a lot of care. Experiment design and the input sequence are a whole other topic. Data collection, sensors, and the environment are other requirements that can sometimes be very expensive and out of reach. Time is also an important factor to consider. Thus, the need for a faster and cheaper process, even if it compromises the accuracy, is necessary at least for the prototype stage.

Froude Scaling is novel a technique that suggests scaling the dynamics of one multirotor to another. The original paper suggests computing the dimensionless Froude Number as the ratio between a selected dimension of the reference multirotor to the target one. In this research, the uncertain models of 4 multirotors were scaled and analyzed, then compared to the true model through the frequency response and eigenvalue locations. The closed-loop response was also evaluated and analyzed using Robust Control which was optimized using the $H_\infty$ synthesis algorithm.

The Froude Scaling idea is appealing and interesting, being able to approximate the location of poles/zeros of the model without even running the rotors is powerful. However, the study concludes that the Dimensionless Froude Number cannot be enough to describe the variability between the multirotors. Other factors like the configuration (the way the rotors are set up) and the number of rotors can be of huge effect. It was already concluded[6] that changing the configuration does not change the dynamics, however, it does change the control authority since the number of rotors to perform a task is different.

Before trying to scale the dynamics, one needs to understand how the size, number of rotors, and change in configuration may affect the dynamics. Then the models can be scaled based on those factors accordingly.

**Keywords:** Froude Scaling, Froude Number, Model Scaling, Optimal Control, $H_\infty$ Synthesis.

# Abstract (Italiano)

Al giorno d'oggi, l'interesse per gli Unmanned Aerial Vehicles (UAV) multirotore è aumentato esponenzialmente[5] in varie applicazioni militari e civili; queste attività richiedono requisiti di alto livello da soddisfare mediante la progettazione di leggi di controllo robuste e ad alte prestazioni, che di solito si basano sulla modellazione fisica del sistema: la scienza della costruzione di modelli matematici di processi dinamici a partire da dati sperimentali é chiamata "identificazione del sistema" e svolge un ruolo significativo. Gli strumenti di identificazione del modello sono ampiamente disponibili al giorno d'oggi. L'argomento è abbastanza maturo per identificare i modelli con grande certezza. Tuttavia, il processo non è neanche lontanamente accessibile e richiede molta cura. La progettazione dell'esperimento e la sequenza di input sono altre questioni problematiche. La raccolta dei dati, i sensori e l'ambiente sono altri requisiti che a volte possono essere molto costosi e fuori portata. Anche il tempo è un fattore importante da considerare. Pertanto, c'é la necessità di un processo più rapido ed economico, anche se compromette l'accuratezza, almeno per la fase di prototipazione.

Froude Scaling è una nuova tecnica che suggerisce di ridimensionare le dinamiche di un multirotore a un altro. Il documento originale suggerisce di calcolare il numero di Froude adimensionale come il rapporto tra una dimensione selezionata del multirotore di riferimento e quella di destinazione. In questa ricerca, i modelli incerti di 4 multirotori sono stati scalati e analizzati, quindi confrontati con il modello reale attraverso la risposta in frequenza e le posizioni degli autovalori. Anche la risposta a circuito chiuso è stata valutata e analizzata utilizzando Robust Control che è stato ottimizzato utilizzando l'algoritmo di sintesi $H_\infty$.

L'idea di Froude Scaling è allettante e interessante, dato che, essere in grado di approssimare la posizione dei poles/zeros del modello senza nemmeno far funzionare i rotori è potente. Tuttavia, lo studio conclude che il Dimensionless Froude Number non può essere sufficiente per descrivere la variabilità tra i multirotori. Altri fattori come la configurazione (il modo in cui sono installati i rotori) e il numero di rotori possono avere

un effetto enorme. È già stato concluso[6] che cambiare la configurazione non cambia le dinamiche, tuttavia, cambia l'autorità di controllo poiché il numero di rotori per eseguire un compito è diverso.

Prima di provare a scalare le dinamiche, è necessario capire in che modo le dimensioni, il numero di rotori e il cambiamento di configurazione possono influire sulle dinamiche. Di conseguenza i modelli possono essere ridimensionati in base a tali fattori.

**Parole chiave:** Froude Scaling, Froude Number, Model Scaling, Optimal Control, $H_\infty$ Synthesis.

# Contents

# List of Figures

# List of Tables

# Introduction

In the design process of new aircraft the development of mathematical models able to predict the vehicle's dynamic behavior is a necessary since it gives the ability to assess safety and quality control of the vehicle. The main objective of having a mathematical model is to develop a model-based controller that could be implemented in the vehicle to achieve certain stability and performance objectives.

A mathematical model is said to be accurate if it is able to predict the relevant dynamics over the time scales and the frequency ranges of interest. The high level of accuracy is required in this process to be able to design a control system that can be considered robust. The process through which it is possible to obtain these models is system identification; first of all an experimental test is performed and data is collected, where an input provides excitation to the system, and then the outputs are measured and stored. Afterwards, using model identification algorithms, a mathematical model able to predict the measured dynamics is derived.

System identification is a well developed topic in the industry, however, the process can be very expensive and sometimes out of reach. Dedicated labs and high quality sensor are indeed needed in order to capture the output dynamics accurately. The system identification process can also be time consuming if the model design is iterated multiple time, i.e., identifying the model each time a modification in the design is done. This can be impractical, and the need for quicker, more affordable ways to predict the underlying mathematical model is increasing. A complementary approach includes new techniques which allow to utilize an identified mathematical model of one multirotor vehicle to extrapolate the dynamics to larger/smaller scale. This is especially important when considering control system design and handling quality metrics, for which it would be important to be able to scale as opposed to developing new metrics for every possible vehicle size class. This procedure is carried out by scaling an identified model used as reference to obtain directly a scaled model representative of the dynamics of another multirotor, through the use of an non-dimensional number called Froude number, that allows to compute some

designated parameters of the predicted model; the scaling factors are different for each parameter and they are based on dimensional considerations.

The model scaling idea will forever change the multirotor industry. Imagine not only scaling a model for the new multirotor and designing the control system, but it could be used the other way around as well. It could be included in the preliminary design process by setting specific model qualities and design the multirotor accordingly. Unfortunately, the scaling is much more complicated than just using the Froude number based on one parameter that depends on the size of the vehicle. Other design parameters such as the rotor configuration and number of rotors must be included in the equation for a better chance to find a a scaling factor that can fit all cases.

Finally, the aim of this thesis is to prove the validity of the Froude technique, then, to analyze the effectiveness of the technique and suggest what should be taken into account in future studies, focusing on the lateral dynamics of four small-scale multirotors UAVs with different configurations.

# 1 | The drones used in the study

In this chapter, we will go through the drones used in the study one by one, and explore their properties, similarities as well as differences.

## 1.1. ANT-R quadrotor[4]

ANT-R(see Figure 1.1) is a light racer quadrotor with high performance and optimized for forward flight; it is composed of commercial off-the-shelf components (see Figure 4.2). Its main features are reported in Table-1.1

| | |
|---|---|
| **Take off mass** | 838 g |
| **Frame size** | $0.18m \times 0.20m \times 0.04m$ |
| **Diameter (motor-to-motor distance)** | 0.26 m |
| **Lateral distance (between rotors hubs centers)** | 0.18 m |
| **Rotor configuration** | H-shaped |
| **Battery** | 4S Li-Po 2650 mAh |
| **Flight time (hovering)** | 13 min |

Table 1.1: Features of ANT-R Quadcopter

Due to its H-shaped asymmetric configuration, the inertia moments around the X-body and Y-body axes are different.

The useful physical parameters for the Froude scaling technique are the total mass (838g), the lateral distance between the rotor hubs (18cm), and the diagonal distance between the rotor hubs (26 cm).

Figure 1.1: ANT-R quadrotor

## 1.2. ANT-X quadrotor[4]

ANT-X (see Figure 1.2) is a small quadrotor equipped with an external structure that contains the rotors and the UAV itself (see Figure 4.3). Its main features are reported in Table-1.2.

| | |
|---|---|
| **Take off mass** | 307 g |
| **Frame size** | $0.20m \times 0.20m \times 0.04m$ |
| **Diameter (motor-to-motor distance)** | 0.16 m |
| **Lateral distance (between rotors hubs centers)** | 0.12 m |
| **Rotor configuration** | X-shaped |
| **Battery** | 3S Li-Po 950 mAh |
| **Flight time (hovering)** | 6.5 min |

Table 1.2: Features of ANT-X Quadcopter

Unlike the ANT-R quadrotor, the ANT-X configuration is symmetric (i.e., the lateral dimension is equal to the longitudinal dimension) and hence the inertia moments about the X-body and Y-body axes are equal.

The useful physical parameters for the Froude scaling technique are the total mass (307

g), the lateral distance between the rotor hubs (12 cm), and the diagonal distance between the rotor hubs (16 cm).

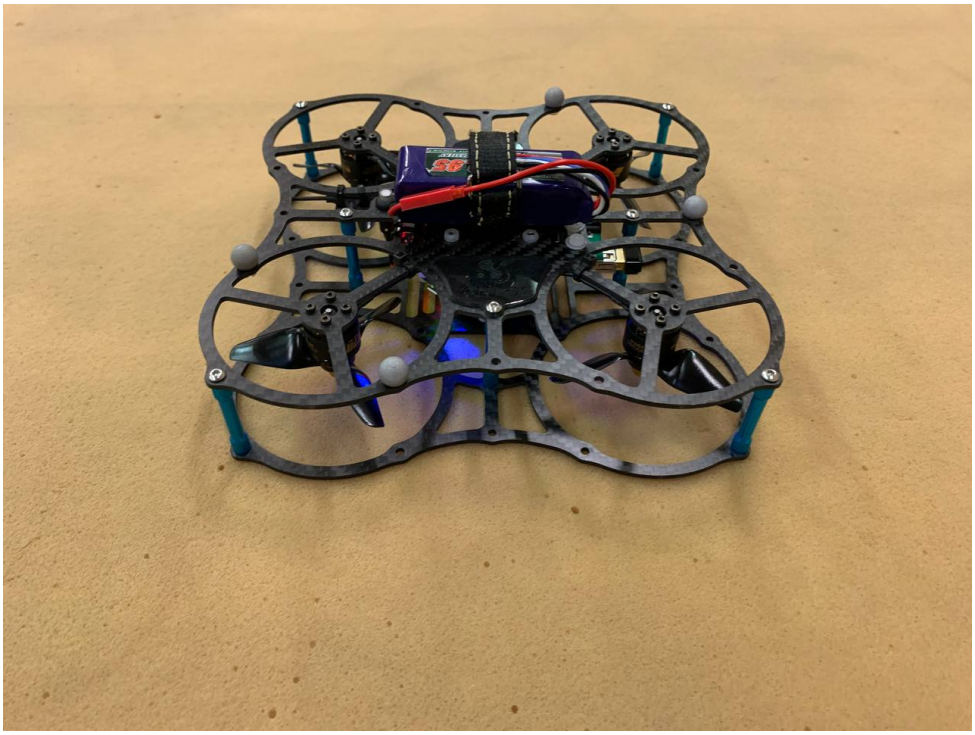

Figure 1.2: ANT-X quadrotor.

## 1.3. CARRIER-1 Octarotor[4]

The CARRIER-1 multirotor (see Figure 1.3) differs from the others used for its configuration since it is an octarotor (i.e., it has eight rotors); its main features are reported in Table-1.3.

| | |
|---|---|
| **Take off mass** | 2563 g |
| **Frame size** | $0.58m \times 0.58m \times 0.14m$ |
| **Diameter (motor-to-motor distance)** | 0.55 m |
| **Lateral distance (between rotors hubs centers)** | 0.40 m |
| **Rotor configuration** | octacopter configuration |
| **Battery** | 6S Li-Po 8000 mAh |
| **Flight time (hovering)** | 16 min |

Table 1.3: Features of CARRIER-1 Octacopter

The same considerations made for the ANT-X quadrotor can be made since both multi-rotors are symmetric. Regarding the Froude scaling, the useful physical parameters are the total mass (2563 g), the lateral distance between the rotor hubs (40 cm), and the diagonal distance between the rotor hubs (55 cm).

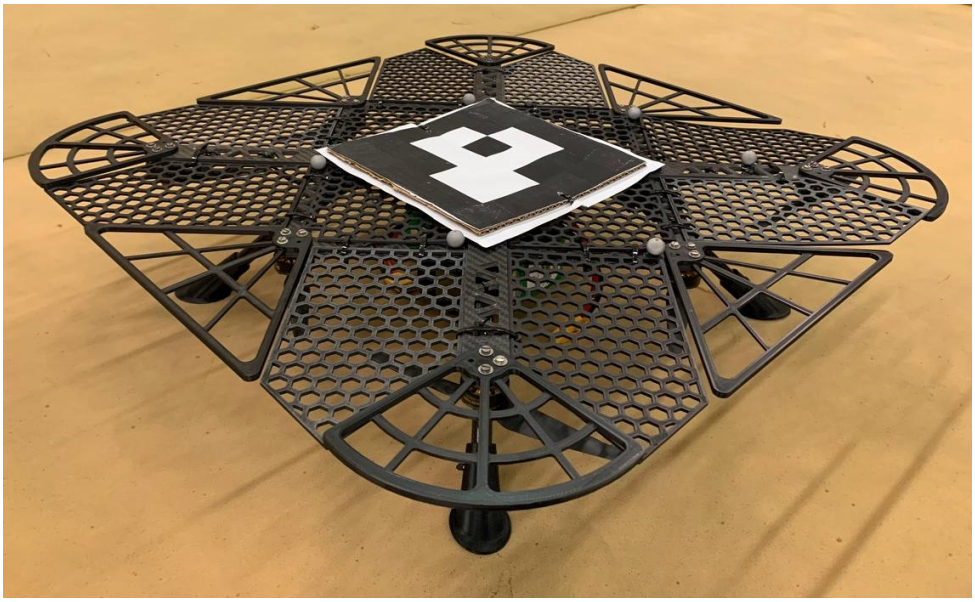

Figure 1.3: CARRIER-1 octarotor

## 1.4. ADAM-0 quadrotor[4]

The ADAM-0 (see Figure 1.4) quadrotor is considered (see Figure 4.5); its main features are reported in Table-1.4

| | |
|---|---|
| **Take off mass** | 1388 g |
| **Frame size** | $0.40m \times 0.40m \times 0.08m$ |
| **Diameter (motor-to-motor distance)** | 0.55m |
| **Lateral distance (between rotors hubs centers)** | 0.40m |
| **Rotor configuration** | X-shaped |
| **Battery** | 3S Li-Po 4000 mAh |
| **Flight time (hovering)** | 10 min |

Table 1.4: Features of ADAM-0 Quadcopter

It can be noted that the CARRIER-1 octarotor and the ADAM-0 quadrotor have the same dimensions in terms of lateral, longitudinal, and thus the diagonal distance between the rotors, but their different configuration will make their comparison more significant, especially in the application of the Froude scaling technique.

Eventually, the useful physical parameters for the dynamic scaling application are the total mass (1388 g), the lateral distance between the rotor hubs (40 cm), and the diagonal distance between the rotor hubs (56 cm).

Figure 1.4: ADAM-0 quadrotor.

# 2 | Identified lateral dynamics model

In this study, only the lateral dynamics have been considered, each vehicle's dynamics were identified independently, and thus it is safe to assume that there is no correlation caused by the identification process, and all the correlation is either caused by the choice of model and/or reality.

All vehicles were identified using a structure, be it a transfer function or a state space system, both identification processes aim at estimating the control derivatives within the structure. In the next sections, each vehicle will be presented with its identified model.

## 2.1. $PBSID_{opt}$-$H_\infty$ identification

Model identification is the practice of building a mathematical model (transfer functions / state-space models) from experimental data collected in the time/frequency domain either in open-loop or closed-loop. The drones used in this study were identified in closed-loop, since the lateral dynamics are not stable, using $PBSID_{opt}$-$H_\infty$ (see [1]) which is a technique that uses Predictor-Based Subspace Identification (PBSID) which is a black-box identification algorithm, and combines it with $H_\infty$ which is a structured, physically motivated model identification algorithm to obtain a structured model that describes the psychical parameters of the lateral dynamics, namely the stability and control derivatives (see reference [4]).

The $PBSID_{opt}$ identification was done using the PBSID toolbox which was developed by Technische Universiteit Delft researchers as an implementation of utilities for system identification with PBSID algorithms in the MATLAB® environment. While the $H_\infty$ model matching was done by solving an optimization problem (see equation (2.1)), minimizing the norm of the difference of the response of the unstructured model and the structured one. The set of parameters that minimize the norm is set to define the values

of the structured model, mostly chosen as stability and control derivatives, which have a clear physical meaning.

$$\min_{\theta} \| \hat{G}_{PBSID_{opt}}(s) - G_s(s,\theta) \|_{\infty} \tag{2.1}$$

where, $\hat{G}_{PBSID_{opt}}(s)$ is the transfer function identified using the PBSID algorithm, which is usually of a higher order than the structured model transfer function, $G_s(s,\theta)$. The structured model has two outputs $p, a_y$, roll rate, and lateral acceleration, respectively, and one input $\delta_{lat}$, which leaves us with two transfer functions, as shown in Equations-2.2:

$$\frac{p}{\delta_{lat}} = \frac{s(L_\delta s - L_\delta Y_v + L_v Y_\delta)}{s^3 - (L_p + Y_v)s^2 + (L_p Y_v - L_v Y_p)s - gL_v}\,, \tag{2.2a}$$

$$\frac{a_y}{\delta_{lat}} = \frac{Y_\delta s^3 + (L_\delta Y_p - L_p Y_\delta)s^2 + (L_\delta Y_v - L_v Y_\delta)g}{s^3 - (L_p + Y_v)s^2 + (L_p Y_v - L_v Y_p)s - gL_v}\,. \tag{2.2b}$$

The state-space representation of the system is given in Equations-2.3 and its parameters are shown in Table-2.1

$$\begin{Bmatrix} \dot{v} \\ \dot{p} \\ \dot{\phi} \end{Bmatrix} = \begin{bmatrix} Y_v & Y_p & g \\ L_v & L_p & 0 \\ 0 & 1 & 0 \end{bmatrix} \begin{Bmatrix} v \\ p \\ \phi \end{Bmatrix} + \begin{bmatrix} Y_\delta \\ L_\delta \\ 0 \end{bmatrix} \delta_{lat}\,, \tag{2.3a}$$

$$\begin{Bmatrix} p \\ a_y \end{Bmatrix} = \begin{bmatrix} 0 & 1 & 0 \\ Y_v & Y_p & 0 \end{bmatrix} \begin{Bmatrix} v \\ p \\ \phi \end{Bmatrix} + \begin{bmatrix} 0 \\ Y_\delta \end{bmatrix} \delta_{lat}\,. \tag{2.3b}$$

Table-2.1 shows the identified structural model parameters, i.e. stability and control derivatives, with the corresponding uncertainties. The red-colored standard deviation indicates poor accuracy with respect to the other parameters, while the red-colored parameters indicate that there is a fundamental disagreement between the stability/control derivatives of at least one drone which is caused by having opposite signs. The table also shows that the ANT-X model is the most confident of all, and it must be due to the experimental excitation which happened to excite the dynamics more and give a better quality response, in general, the models are considered good enough to describe the dynamics of

the corresponding drones.

| | ANT-R | ANT-X | CARRIER-1 | ADAM-0 |
|---|---|---|---|---|
| $Y_v$ | $-0.26 \pm 2.74\%$ | $-0.1068 \pm 4.26\%$ | $-0.4732 \pm 6.47\%$ | $-0.5945 \pm 14.83\%$ |
| $Y_p$ | $0.0296 \pm 12.2\%$ | $0.1192 \pm 2.03\%$ | $-0.0852 \pm 27.21\%$ | $-0.2047 \pm 32.71\%$ |
| $Y_d$ | $10.1566 \pm 4.63\%$ | $-10.1647 \pm 1.37\%$ | $4.4423 \pm 6.84\%$ | $10.8255 \pm 2.84\%$ |
| $L_v$ | $-7.3708 \pm 3.05\%$ | $-5.9755 \pm 1.83\%$ | $-5.5668 \pm 5.94\%$ | $-5.1977 \pm 6.1\%$ |
| $L_p$ | $0.2153 \pm 52.7\%$ | $-2.6478 \pm 2.01\%$ | $-2.5041 \pm 7.26\%$ | $-0.4555 \pm 21.95\%$ |
| $L_d$ | $1150.6 \pm 1.45\%$ | $450.71 \pm 0.81\%$ | $229.4410 \pm 3.29\%$ | $186.8301 \pm 3.62\%$ |

Table 2.1: Identified Structured Model Parameters with Uncertainty.

## 2.2. Lateral dynamics block diagram

The block diagram of the lateral dynamics consists of an active Stability and Control Augmentation System. The inner loop is what is called the "Roll Damper" which tracks the roll rate set-point, while the outer loop is the "Attitude Hold" which tries to track a roll angle set-point.

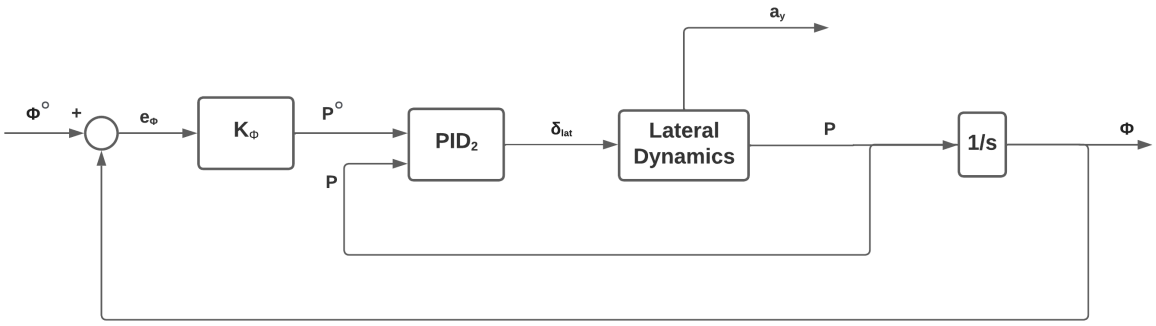


Figure 2.1: Lateral Dynamics Block Diagram.

Table-2.2 shows the gains used in the stability and control augmentation loop during the flight tests[4]. These gains will be used later to validate the scaled models in closed-loop.

**PID gains and Roll proportion gain**

| Gain | ANT-X | ANT-R | CARRIER-1 | ADAM-0 |
|---|---|---|---|---|
| $K_\phi$ | 6.5 | 10 | 6.5 | 6.5 |
| $K_P$ | 0.05 | 0.08 | 0.15 | 0.15 |
| $K_I$ | 0.05 | 0.05 | 0.2 | 0.05 |
| $K_D$ | 0.001 | 0.0015 | 0.002 | 0.003 |

Table 2.2: Controllers' gains used in flight tests.

# 3 | Open-loop response of the lateral dynamics

In this chapter, the response of the lateral dynamics (only roll rate) will be studied. A comparison between the different vehicles in terms of frequency domain response and eigenvalues will be carried out. Time-domain comparison is not possible in this context since all systems are open-loop unstable. All vehicles have a frequency range of interest around 1-50 rad/s which will be taken into account when comparing the responses.

The lateral dynamics generally consist of 2 modes, real-valued Roll mode, and complex-conjugate phugoid mode, which will be studied separately.

## 3.1. Frequency response - Bode plot

The Bode plot (see Figure 3.1) shows the frequency response of each system and how they differ. It is known that all systems have at least one unstable mode. The plot also shows that the vehicles' lateral dynamics do not differ very much, in fact, all systems agree on the behavior in general, while the peak frequency, damping ratio, and magnitude are expected to be different.

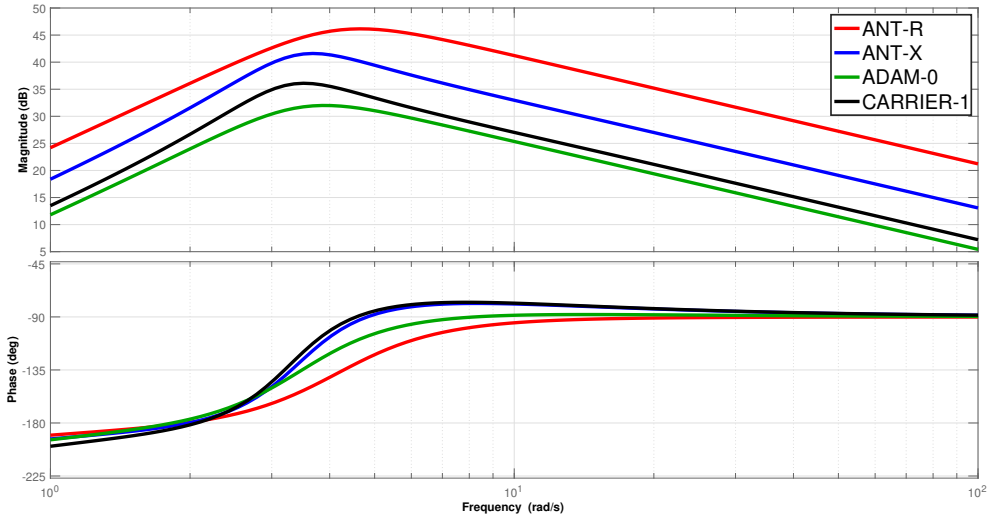


Figure 3.1: Frequency Response of Lateral Dynamics $\delta_{lat}$ to $p$.

## 3.2. Eigenvalues of the Open Loop Dynamics

The lateral dynamics, consist of 2 different modes, roll subsidence and phugoid modes. Both modes will be discussed and compared in this section.

Figure 3.2 shows the placement of the eigenvalues of each drone. It is very clear that all four drones have similar dynamic responses. For example, ANT-R (red) and ADAM-0 (GREEN) almost exactly agree when it comes to the Roll mode, while they differ a bit when it comes to the phugoid damping ratio.

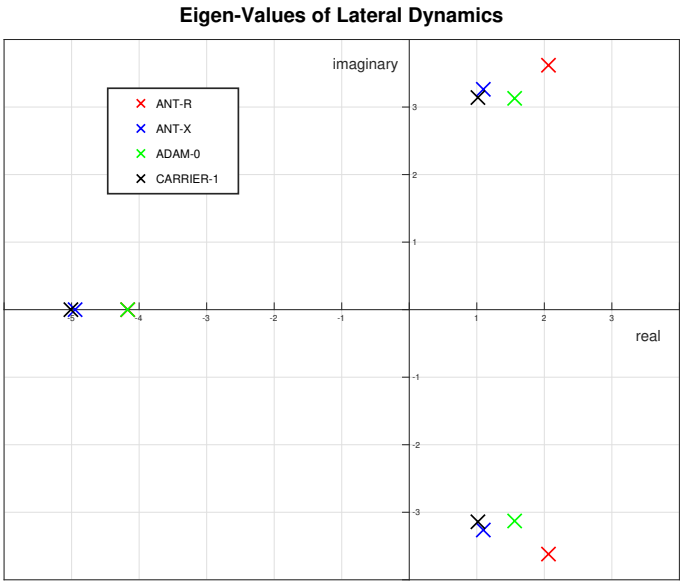


Figure 3.2: Eigenvalues of Lateral Dynamics $\delta_{lat}$ to $p$.

Table-3.1 shows the natural frequency and damping ratios for each lateral mode for all 4 vehicles. All vehicles have a stable roll mode, which is expected.

It is also important to notice that all modes have frequencies of the same order of magnitude, and follow the same pattern. This is also evident from the frequency response (see Figure 3.1) and the eigenvalues (see Figure 3.2) of the systems which shows how close the behavior between the systems is.

**Eigenvalues (poles) of the lateral dynamics**

| | **Roll** | | **Dutch Roll** | |
|---|---|---|---|---|
| | $\omega_n$ (rad/s) | $\zeta$ | $\omega_n$ (rad/s) | $\zeta$ |
| **ANT-R** | 4.17 | 1 | 4.17 | -0.495 |
| **ADAM-0** | 4.17 | 1 | 3.5 | -0.446 |
| **ANT-X** | 4.95 | 1 | 3.44 | -0.319 |
| **CARRIER-1** | 5.01 | 1 | 3.30 | -0.308 |

Table 3.1: Comparison of the eigenvalues between the different vehicles.

# 4 | Froude scaling technique

## 4.1. Introduction

The system identification tools/algorithms have been developed over the years, however, the cost and time to make practical, high-quality experiments to collect data is still high, and that is where dynamic scaling comes in handy.

The Froude Scaling is a novel idea that allows researchers to find an approximate, good-enough model that describes the dynamics of the target system which is nothing but a scaled model of an already identified and validated model of another multirotor vehicle. This is generally a good option since the model is usually needed only to design a model-based controller with specific response requirements (handling qualities).

Scaling is accomplished using the so-called Froude Number, which is a ratio between a geometric characteristic of the two multirotors, reference-to-target ratio (see equation (4.1)).

$$N = \frac{L_{reference}}{L_{targer}} \tag{4.1}$$

In the next section, the process of scaling stability and control derivatives (see reference [2]) is reported.

## 4.2. Froude Scaling Process

As already mentioned, the Froude Scaling is done through the Froude Number (see equation (4.1)). It was suggested to use the Hub-to-Hub distance as the reference length (see reference [2]) to scale the stability and control derivatives. Table 4.1 shows the scaling factor for each parameter with respect to its own unit.

**Scaling Factors of Control and Stability Derivatives**

| Derivative | Unit | Scaling Factor |
|---|---|---|
| $Y_v$ | $\frac{1}{s}$ | $\sqrt{N}$ |
| $Y_p$ | $\frac{m}{s \cdot rad}$ | $\frac{\sqrt{N}}{N}$ |
| $Y_\delta$ | $\frac{m}{s^2}$ | / |
| $L_v$ | $\frac{rad}{m \cdot s}$ | $N\sqrt{N}$ |
| $L_p$ | $\frac{1}{s}$ | $\sqrt{N}$ |
| $L_\delta$ | $\frac{rad}{s^2}$ | N |

Table 4.1: Stability and control derivatives unit of measure and scaling factor.

This method of scaling the stability and control derivatives was suggested in [2] which is not necessarily the best option, however, it will be discussed and analyzed for the sake of completeness. Then, a stochastic eigen-value scaling method will be presented which gives better, and more realistic results.

# 5 | Froude scaling - deterministic approach

As mentioned in the previous chapter (Chapter 4), the Froude Scaling is meant to give an approximate, good-enough model that describes the dynamics of the target multirotor.

The original authors[2] suggested that the scaling should be done by using the scaling factors in Table-4.1 with the reference length (see equation (4.1)) being the Hub-to-Hub distance.

In the following sections, the exact mentioned process will be used to assess the accuracy of the scaled model. Note that from here on, the models identified by Lizza[4] will be taken for granted as the "true" model, thus, no non-parametric data will be dealt with.

## 5.1. ANT-R as Target

In this section, the ANT-R drone will be used as a target, and all other 3 drones, namely, ANT-X, ADAM-0, and CARRIER-1 will be scaled to approximate the ANT-R dynamics.

The following table shows the Froude Number calculated as the Hub-to-Hub distance of the reference drones to the length of the ANT-R.

| Multirotor | Hub-to-Hub distance | Froude Number (N) |
|---|---|---|
| **ANT-R** | 0.26m | 1 |
| **ANT-X** | 0.16m | 0.6154 |
| **ADAM-0** | 0.55m | 2.1154 |
| **CARRIER-1** | 0.55m | 2.1154 |

Table 5.1: Froude Number of the multirotors with respect to ANT-R.

Note that ANT-X is about two-thirds of ANT-R, while ADAM-0 and CARRIER-1 are more than twice ANT-R.

The scaled stability and control derivatives are mentioned in table-5.2, it is possible to see that there is a clear mismatch between the derivatives, especially the sign, which is somehow expected given that each drone has a different configurations, structure, number of rotors, etc.

| | **ANT-R** (true) | **ANT-X** (scaled) | **CARRIER-1** (scaled) | **ADAM-0** (scaled) |
|---|---|---|---|---|
| $Y_v$ | $-0.26$ | $-0.0838$ | $-0.6882$ | $-0.8647$ |
| $Y_p$ | 0.0296 | 0.1520 | $-0.0586$ | $-0.1407$ |
| $Y_d$ | 10.1566 | $-10.1650$ | 4.4423 | 10.8255 |
| $L_v$ | $-7.3708$ | $-2.8847$ | $-17.1273$ | $-15.9917$ |
| $L_p$ | 0.2153 | $-2.0771$ | $-3.6421$ | $-0.6625$ |
| $L_d$ | 1150.6 | 277.3600 | 485.3538 | 395.2175 |

Table 5.2: comparing the stability and control derivatives of the true ANT-R model to the scaled model.

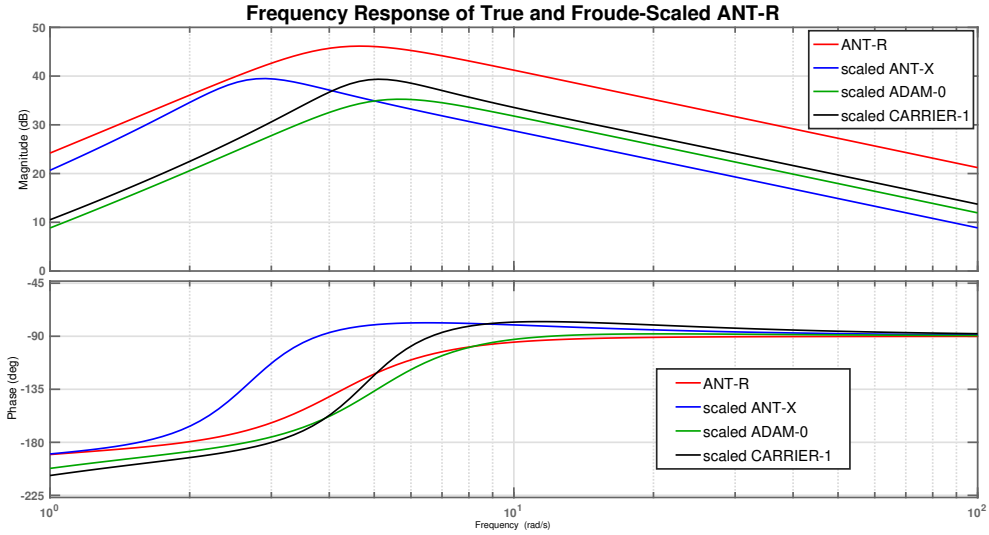


Figure 5.1: Frequency Response of True and Froude-Scaled ANT-R Lateral Dynamics $\delta_{lat}$ to $p$.

Now, the eigenvalues and frequency response shall be compared, Figures (5.1, 5.2) show the frequency response of the true and scaled models as well as their eigenvalues (poles).

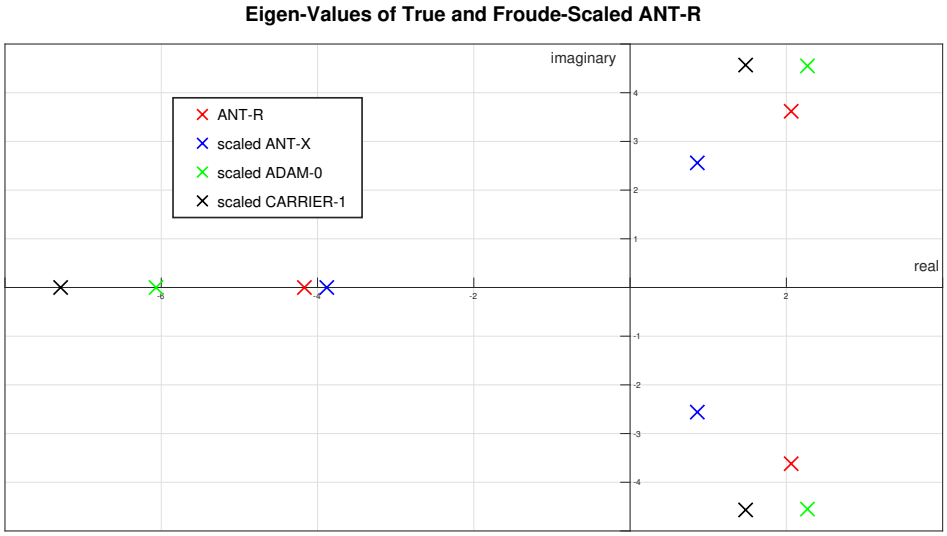


Figure 5.2: Eigenvalues of True and Froude-Scaled ANT-R Lateral Dynamics $\delta_{lat}$ to $p$.

Both figures show that the scaled models are not approximating the true one very well, in fact, there is barely an improvement from the original multirotor dynamics, which is not enough to conclude anything.

Now let's analyze the ANT-X multirotor and see if different results can be found.

## 5.2. ANT-X as Target

This time, the ANT-X drone will be used as a target, and all other 3 drones, namely, ANT-R, ADAM-0, and CARRIER-1 will be scaled to approximate the ANT-X lateral dynamics.

The following table shows the Froude Number calculated as the Hub-to-Hub distance of the reference drones to the target ANT-X.

| Multirotor | Hub-to-Hub distance | Froude Number (N) |
|---|---|---|
| **ANT-R** | 0.26m | 1.6250 |
| **ANT-X** | 0.16m | 1 |
| **ADAM-0** | 0.55m | 3.4375 |
| **CARRIER-1** | 0.55m | 3.4375 |

Table 5.3: Froude Number of the multirotors with respect to ANT-X.

The procedure is exactly the same as with the ANT-R in the previous section, the idea is to scale the stability and control derivatives and compare the frequency response and eigenvalues of the scaled models to the true one.

| | ANT-R (scaled) | ANT-X (true) | CARRIER-1 (scaled) | ADAM-0 (scaled) |
|---|---|---|---|---|
| $Y_v$ | $-0.3314$ | $-0.1068$ | $-0.8773$ | $-1.1022$ |
| $Y_p$ | 0.0232 | 0.1192 | $-0.0460$ | $-0.1104$ |
| $Y_d$ | 10.1570 | $-10.165$ | 4.4423 | 10.8255 |
| $L_v$ | $-15.2684$ | $-5.9755$ | $-35.4789$ | $-33.1265$ |
| $L_p$ | 0.2745 | $-2.6478$ | $-4.6427$ | $-0.8445$ |
| $L_d$ | 1869.7 | 450.71 | 788.7 | 642.2285 |

Table 5.4: comparing the stability and control derivatives of the true ANT-X model to the scaled model.

Again, the disagreement is evident, the dynamics are close but very close, and in some cases, the derivatives are getting even further away from the true value instead of getting closer to it.

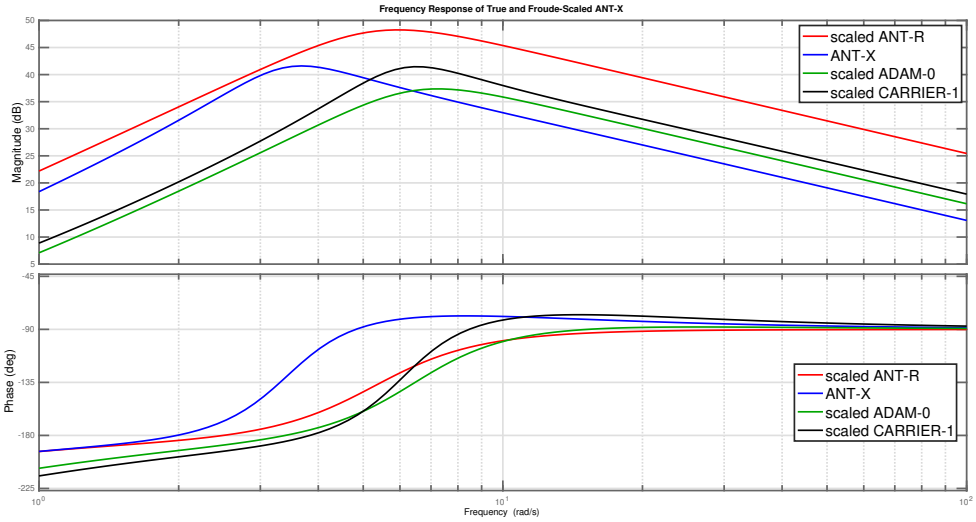


Figure 5.3: Frequency Response of True and Froude-Scaled ANT-X Lateral Dynamics $\delta_{lat}$ to $p$.

The eigenvalues are also spreading away instead of converging to the true value, it will be

more clear when the other two cases are discussed.

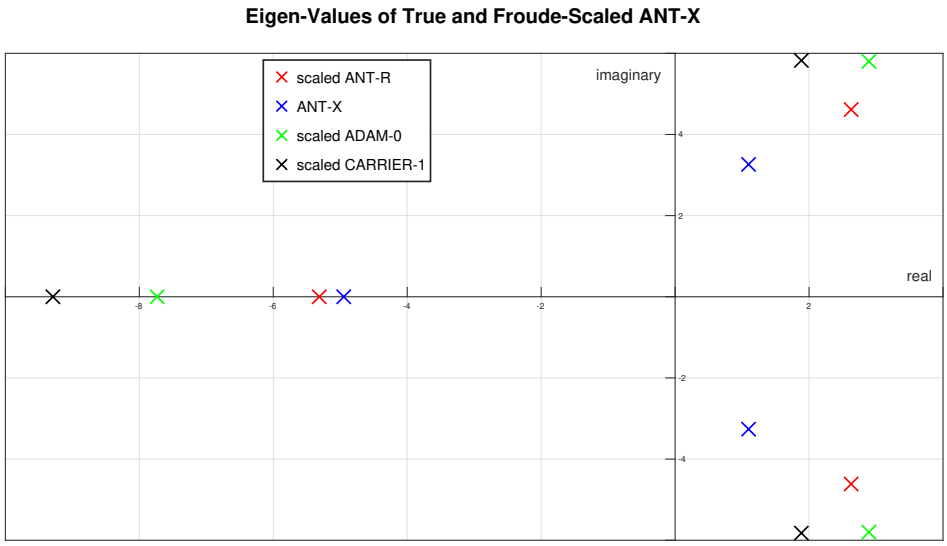


Figure 5.4: Eigenvalues of True and Froude-Scaled ANT-X Lateral Dynamics $\delta_{lat}$ to $p$.

## 5.3. CARRIER-1 as Target

In this section, CARRIER-1 will be taken as the target drone. Keep in mind that the CARRIER-1 and ADAM-0 share the same Hub-to-Hub distance, thus, the Froude Number will be unity (Tables-1.3 and 1.4), and therefore, no scaling will be expected with respect to ADAM-0.

The following table shows the Froude Number calculated as the Hub-to-Hub distance of the reference drones to the target CARRIER-1.

| Multirotor | Hub-to-Hub distance | Froude Number (N) |
|---|---|---|
| **ANT-R** | 0.26m | 0.4727 |
| **ANT-X** | 0.16m | 0.2909 |
| **ADAM-0** | 0.55m | 1 |
| **CARRIER-1** | 0.55m | 1 |

Table 5.5: Froude Number of the multirotors with respect to CARRIER-1.

The exact same metrics will be used, and stability and control derivatives, eigenvalues and frequency response will be compared for true and scaled models.

| | **ANT-R** (scaled) | **ANT-X** (scaled) | **CARRIER-1** (true) | **ADAM-0** (scaled) |
|---|---|---|---|---|
| $Y_v$ | $-0.1788$ | $-0.0576$ | $-0.4732$ | $-0.5945$ |
| $Y_p$ | 0.0431 | 0.2210 | $-0.0460$ | $-0.2047$ |
| $Y_d$ | 10.1570 | $-10.165$ | 4.4423 | 10.8255 |
| $L_v$ | $-2.3957$ | $-0.9376$ | $-5.5668$ | $-5.1977$ |
| $L_p$ | 0.1480 | $-1.4281$ | $-0.4555$ | $-0.8445$ |
| $L_d$ | 543.92 | 131.1156 | 229.44 | 186.8301 |

Table 5.6: comparing the stability and control derivatives of the true CARRIER-1 model to the scaled model.

Even in the case of CARRIER-1, the derivatives do not scale close to the true value, the frequency response is not getting any better than in the previous cases, and the eigenvalues are spreading instead of converging.

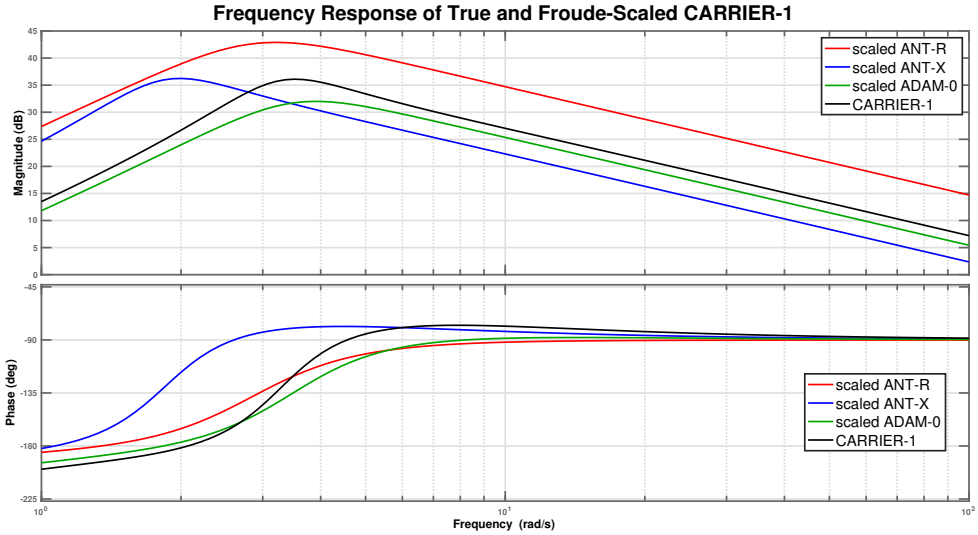


Figure 5.5: Frequency Response of True and Froude-Scaled CARRIER-1 Lateral Dynamics $\delta_{lat}$ to $p$.

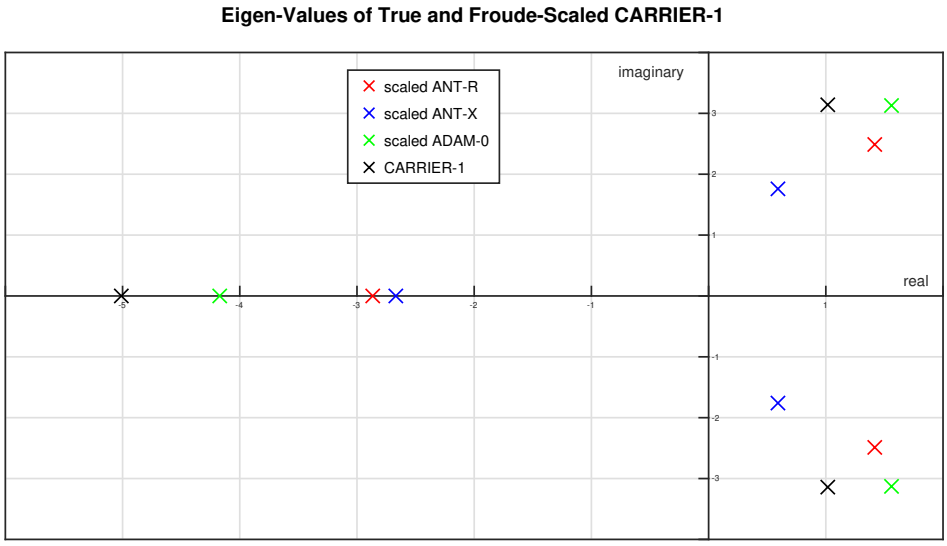


Figure 5.6: Eigenvalues of True and Froude-Scaled CARRIER-1 Lateral Dynamics $\delta_{lat}$ to $p$.

## 5.4. ADAM-0 as Target

Finally, ADAM-0 will be taken as the target drone, and all other three drones' lateral dynamics are scaled according to their respective Froude Number and compared to the

true ADAM-0 model.

The following table shows the Froude Number calculated as the Hub-to-Hub distance of the reference drones to the target ADAM-0.

| Multirotor | Hub-to-Hub distance | Froude Number (N) |
|---|---|---|
| **ANT-R** | 0.26m | 0.4727 |
| **ANT-X** | 0.16m | 0.2909 |
| **ADAM-0** | 0.55m | 1 |
| **CARRIER-1** | 0.55m | 1 |

Table 5.7: Froude Number of the multirotors with respect to ADAM-0.

The stability and control derivatives of the true and scaled models are reported in the following table. Since the ADAM-0 and CARRIER-1 share the same Hub-to-Hub distance, the values are exactly like the ones reported in Table-5.6

| | **ANT-R** (scaled) | **ANT-X** (scaled) | **CARRIER-1** (scaled) | **ADAM-0** (true) |
|---|---|---|---|---|
| $Y_v$ | $-0.1788$ | $-0.0576$ | $-0.4732$ | $-0.5945$ |
| $Y_p$ | 0.0431 | 0.2210 | $-0.0460$ | $-0.2047$ |
| $Y_d$ | 10.1570 | $-10.165$ | 4.4423 | 10.8255 |
| $L_v$ | $-2.3957$ | $-0.9376$ | $-5.5668$ | $-5.1977$ |
| $L_p$ | 0.1480 | $-1.4281$ | $-0.4555$ | $-0.8445$ |
| $L_d$ | 543.92 | 131.1156 | 229.44 | 186.8301 |

Table 5.8: comparing the stability and control derivatives of the true ADAM-0 model to the scaled model.

The frequency response and eigenvalues are, with no surprises, identical to the ones reported in Figure 5.5 and Figure 5.6, respectively.

## 5.5. Conclusion

From the data reported in this chapter, there are a few points to conclude:

1. The Hub-to-Hub distance does not scale the models accurately.
2. In some cases the direction is wrong, i.e. the Froude Number scales the model up ($N > 1$) instead of scaling it down ($N < 1$).
3. The Hub-to-Hub distance predicts the CARRIER-1 and ADAM-0 to be identical, thus, no scaling. The Froude Scaling technique is supposed to be more robust.
4. The eigenvalues are all grouped in a small region, and scaling the models does not make the region smaller, in fact, it makes it larger and spreads the eigenvalues away.

To summarize, the Froude Scaling, introduced in reference[2] is unrealistic in the case of the drones in this study. The idea of scaling a model "deterministically" is in itself unrealistic. When identifying the model using the traditional ways, the result is a model with parametric uncertainty, and therefore the scaled model must also be an uncertain model based on the identified model.

In the next chapter, another approach will be introduced to scale the model with the introduction of model uncertainty. which will bring more insight into the Froude Scaling technique.

# 6 | Froude scaling - uncertainty approach

When identifying a model, uncertainty is an important measurement of how accurate the model is, however, it must remain as low as possible, otherwise the model would not be considered accurate.

In the original Froude Scaling paper[2], it was suggested to scale the model linearly, and certainly. This approach is not realistic, especially after the obtained results confirm that it does not work in the case of the drones of study.

While it is not expected to give exact results, the uncertainty scaling approach is more practical when it comes to identifying a model for control design purposes.

The idea is not to scale the stability and control derivatives but to scale the uncertainty of these parameters, which is the only thing all drones have in common. The eigenvalues consist of two modes, real-valued roll mode, and complex-conjugate dutch roll mode. All drones have comparable frequencies and damping ratios, and the region of interest is small enough to start looking for patterns to scale.

## 6.1. The Location of the Eigenvalues

It is important to study the location of the eigenvalues in the process of finding a way to scale. The lateral dynamics include 2 dominant modes as mentioned, Roll and Dutch Roll.

Figure(6.1) shows the locations of the identified models' eigenvalues of each multirotor, it is clear that all multirotor, despite the size, number of rotors, or weight, have modes that are located within a limited region.

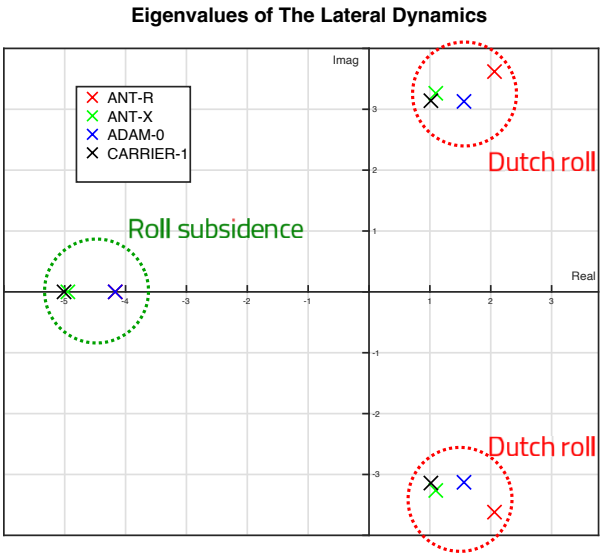


Figure 6.1: Eigenvalues of Identified Lateral Dynamics $\delta_{lat}$ to $p$.

This observation could be limited to the multirotors at hand, however, given the variability of the multirotors, this is an interesting feature to explore.

Also, it is worth mentioning that the eigenvalues do not simply scale correctly by multiplying them by the Froude Number, since the direction is not always correct for all modes.

The eigenvalues determine the behavior of the system. It is noticeable that the eigenvalues spread away (see Figures 5.2, 5.4 and 5.5) instead of converging to the real model (see Figure 6.1). This already makes the approach unfeasible. To understand this more let's do some sensitivity analysis on the eigenvalues of the Froude Number.

## 6.2. Eigenvalues Sensitivity Analysis to The Froude Number

It is crucial to understand how the eigenvalues behave when the stability and control derivatives are scaled. In this section, the four drones will be scaled up and down to understand how the eigenvalues change. Figures 6.2-6.5 show that the scaling is actually one-dimensional, and fails to capture the expected behavior.

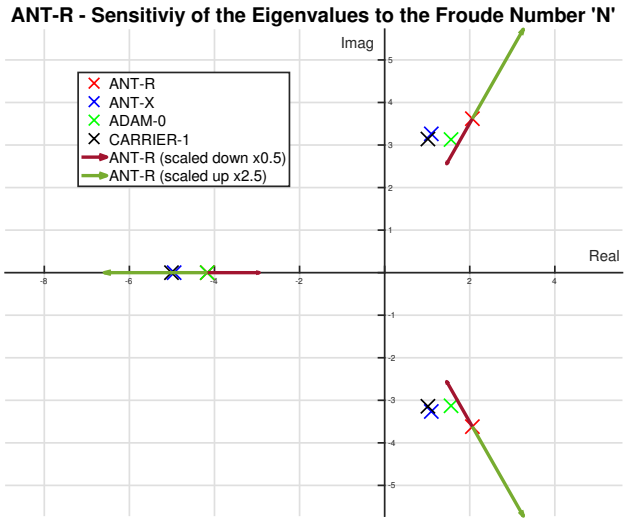


Figure 6.2: Scaling the eigenvalues of ANT-R quadcopter. Green is scaled up and red is scaled down.

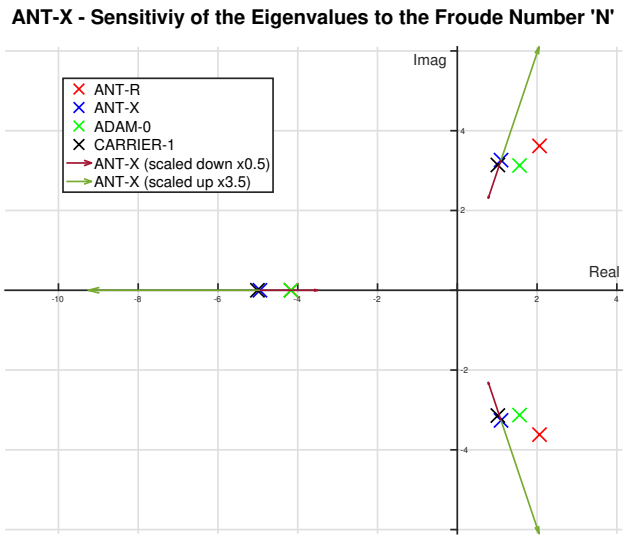


Figure 6.3: Scaling the eigenvalues of ANT-X quadcopter. Green is scaled up and red is scaled down.

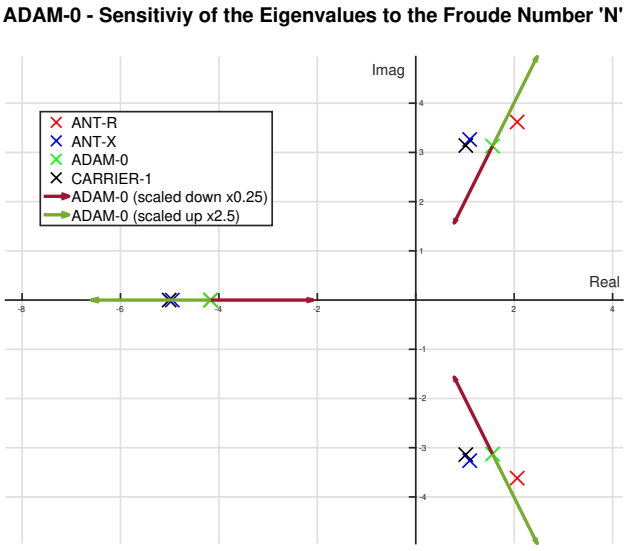


Figure 6.4: Scaling the eigenvalues of ADAM-0 quadcopter. Green is scaled up and red is scaled down.

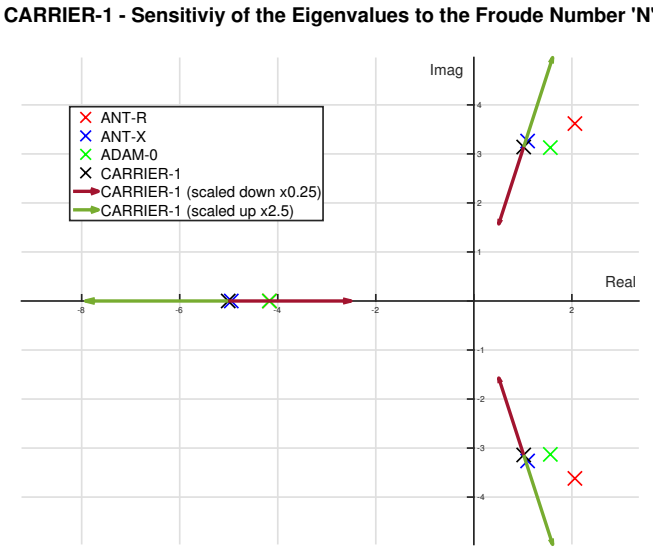


Figure 6.5: Scaling the eigenvalues of CARRIER-1 quadcopter. Green is scaled up and red is scaled down.

It is quite interesting to notice two things, the first observation is that the eigenvalues scale unidirectionally, in one dimension, and along a straight line. This is obvious since both the real and imaginary parts are scaled by the same factor. The second observation is that no matter how large or small the Froude number is, the eigenvalues will never cross the

imaginary axis. This means that the Froude number preserves the structure of the model.

Also, as stated before, it is evident that the ANT-X, for example, is supposed to scale down instead of scaling up, in other words, the ANT-X completely misses the objective of Froude Scaling.

## 6.3. Uncertainty Analysis

The models are uncertain, and the uncertainty is defined by the identified stability and control derivatives (see Table-2.1). This uncertainty does not change the eigenvalues very much (see Figure 6.6). Notice that for the roll subsidence mode, ADAM-0 is very close to ANT-R and ANT-X is almost identical to CARRIER-1.

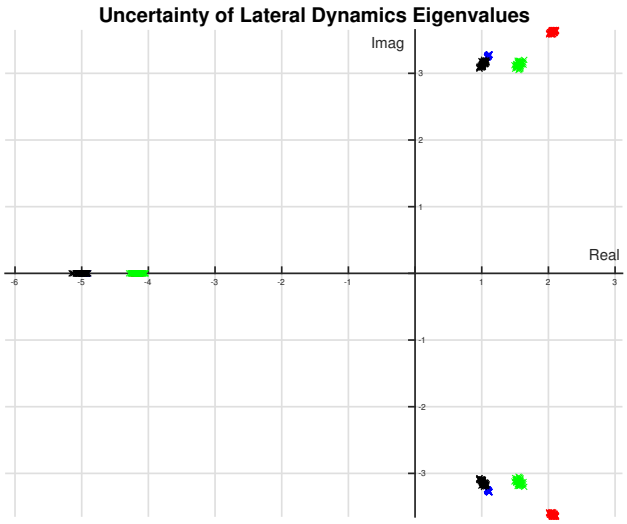


Figure 6.6: Uncertainty of the eigenvalues. Red is ANT-R, blue is ANT-X, green is ADAM-0, and black is CARRIER-1.

The uncertainty is very large for some parameters, however, this uncertainty is not passed on to the eigenvalues. The eigenvalues are located in a very small region, which means that the identification process was done well.

## 6.4. Scaling the Uncertainty

It would be interesting and insightful to see what happens when the parametric uncertainty is scaled. This information will be useful later when designing a controller that

guarantees the performance and stability of the true model based on the scaled model.

### 6.4.1. ANT-R as Target

Here the ANT-R will be used as the target and all other models' uncertainty will be scaled based on the Froude Number, Figure 6.7

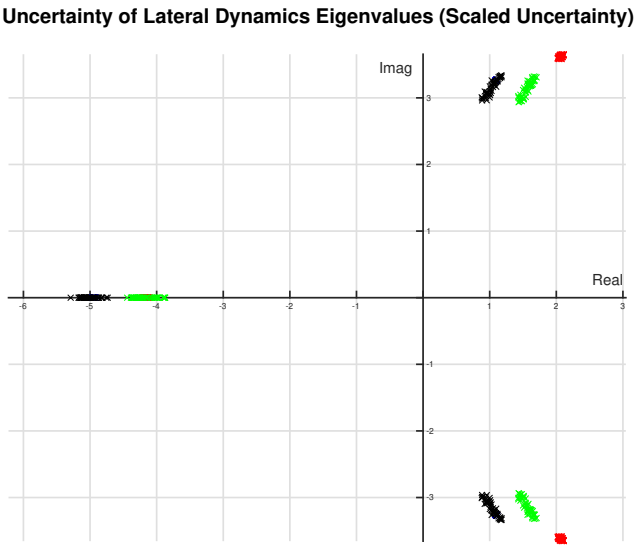


Figure 6.7: Scaled uncertainty of the eigenvalues based on ANT-R. Red is ANT-R, blue is ANT-X, green is ADAM-0, and black is CARRIER-1.

### 6.4.2. ANT-X as Target

Now the ANT-X will be used as the target and all other models' uncertainty will be scaled based on the Froude Number, Figure 6.8

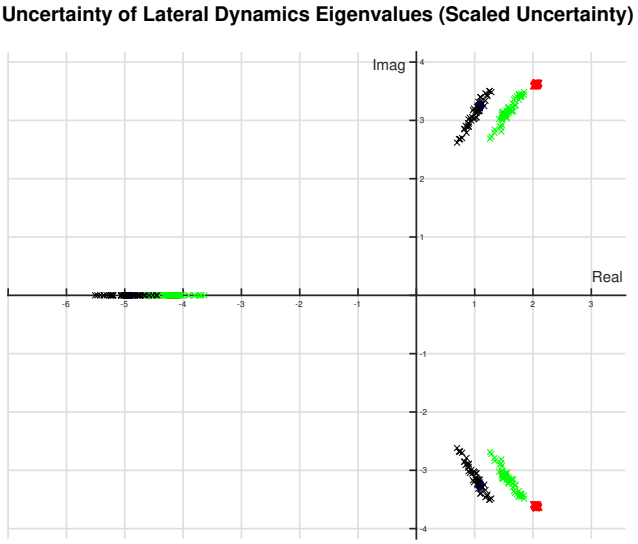


Figure 6.8: Scaled uncertainty of the eigenvalues based on ANT-X. Red is ANT-R, blue is ANT-X, green is ADAM-0, and black is CARRIER-1.

### 6.4.3. CARRIER-1 and ADAM-0 as Target

Now the ADAM-0/CARRIER-1 will be used as the target and all other models' uncertainty will be scaled based on the Froude Number, Figure 6.9

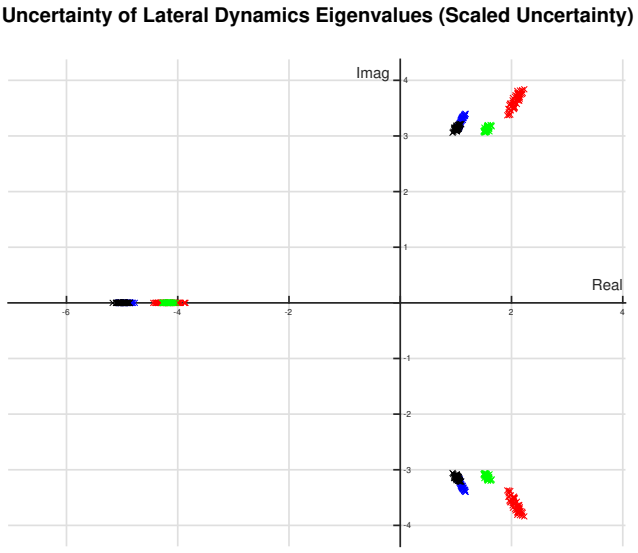


Figure 6.9: Scaled uncertainty of the eigenvalues based on CARRIER-1/ADAM-0. Red is ANT-R, blue is ANT-X, green is ADAM-0, and black is CARRIER-1.

The uncertainty grows, as expected, and the eigenvalues get closer to each other as a result of the growing uncertainty. These results will be useful later for the design of a robust control that respects some requirements.

## 6.5. Scaling the Derivatives and Their Uncertainty

In this section, the parameters will be scaled along with their uncertainty. It will be useful to see how the combination of both will affect the behaviour of the eigenvalues.

### 6.5.1. ANT-R as Target

Here all the models will be scaled according to the ANT-R, manly, the stability and control derivatives and their uncertainty will be scaled. Figure 6.10 shows the scaled eigenvalues.

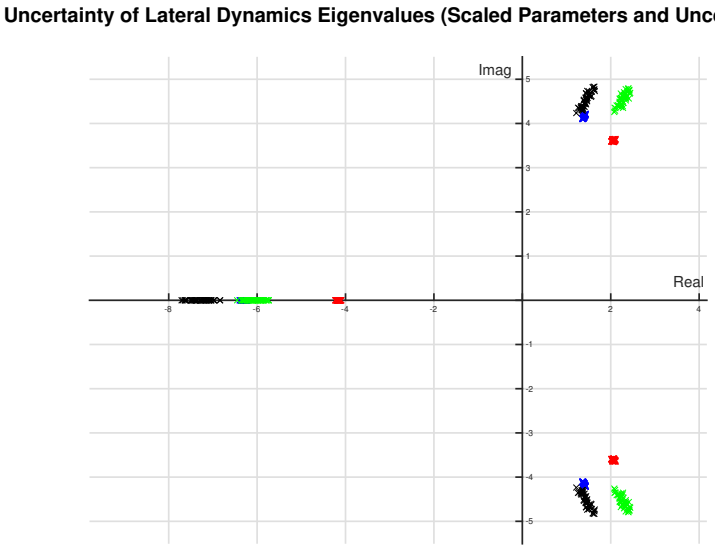


Figure 6.10: Scaled parameters and uncertainty of the model based on ANT-R. Red is ANT-R, blue is ANT-X, green is ADAM-0, and black is CARRIER-1.

Comparing the previous figure to Figure 6.7, no advantage is gained in terms of closeness of the eigenvalues.

### 6.5.2. ANT-X as Target

The models this time will be scaled according to the ANT-X, manly, the stability and control derivatives and their uncertainty will be scaled. Figure 6.11 shows the scaled eigenvalues.

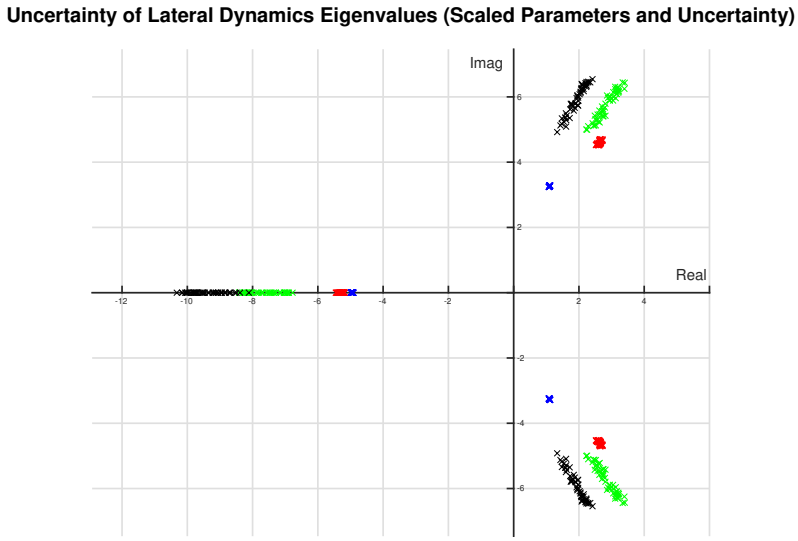


Figure 6.11: Scaled parameters and uncertainty of the model based on ANT-X. Red is ANT-R, blue is ANT-X, green is ADAM-0, and black is CARRIER-1.

### 6.5.3. CARRIER-1 and ADAM-0 as Target

The models this time will be scaled according to the CARRIER-1, manly, the stability and control derivatives and their uncertainty will be scaled. Figure 6.12 shows the scaled eigenvalues.

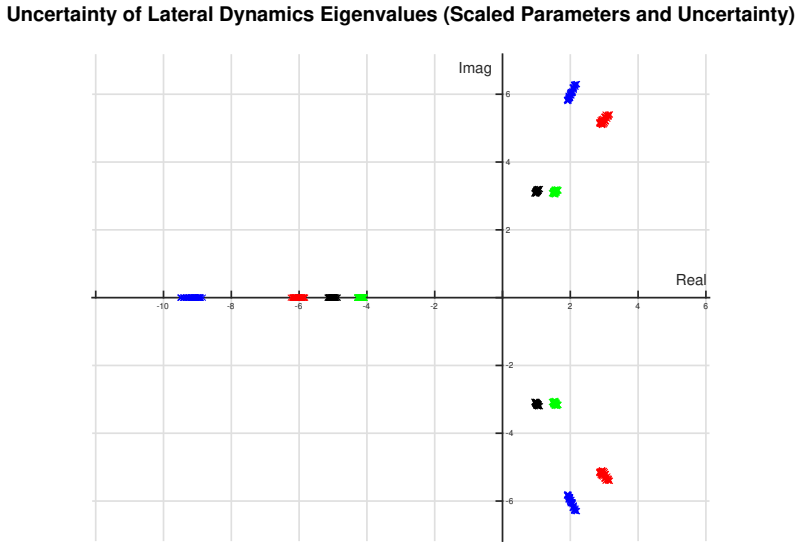


Figure 6.12: Scaled parameters and uncertainty of the model based on CARRIER-1/ADAM-0. Red is ANT-R, blue is ANT-X, green is ADAM-0, and black is CARRIER-1.

In the case of ANT-X, CARRIER-1, and ADAM-0 as targets, the eigenvalues were scaled further away from the true ones. Thus, there is no evidence that the Froude Number is not a general rule for scaling models.

## 6.6. Gain Scaling

The gain of the models is what makes the response different (at least in these 4 multirotors), since the eigenvalues are close enough, the gains are actually not as close and thus the performance can be affected if the controller is designed on the wrong model gains. Figure 6.13

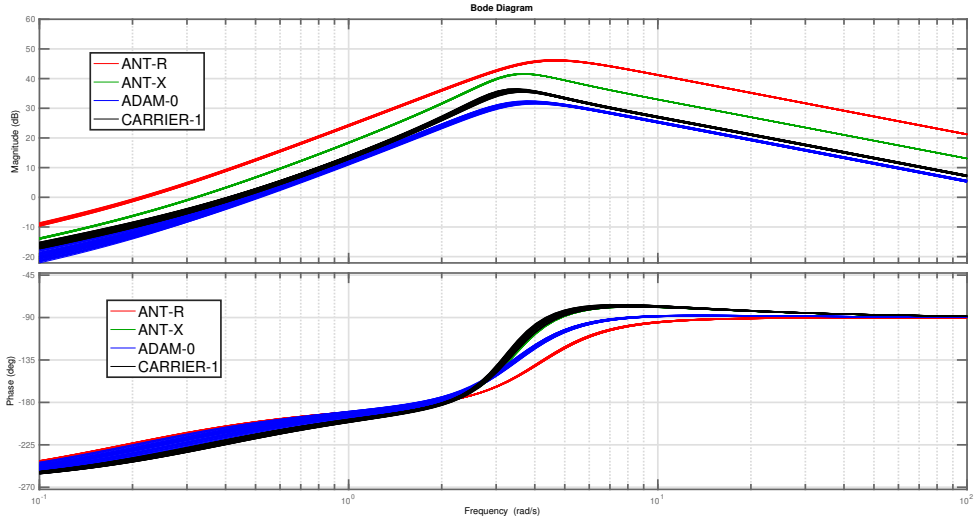


Figure 6.13: The gain and phase plots of uncertain models.

Notice that the phase plot is good, and can be managed by a controller. However, the difference in gains can affect the performance, and sometimes the stability.

It is important to keep a few points into account, the drones have

1. different configurations, X, Plus, Cross, etc.
2. different rotor arrangement, Quad, Hexa, Octa, etc.
3. different structure (perhaps materials)

Robert J. Niemiec and F. Gandhi[6] have done a comparison between two quadcopter configurations, mainly, Plus and Cross configurations. A comparison of the control authority available between the plus- and cross-configuration quadcopters shows that while collective and yaw control authority is identical, pitch and roll control authority is up to about 30% greater for the cross-configuration since all four (as opposed to only two) rotors are used. This suggests that point 1 is to be taken into account. The gain is affected by the difference in configuration while the location of the poles/zero remains identical.

From this, the models will also be scaled by a factor of $\sqrt{N}$ so that the eigenvalues remain the same, while the gain is scaled. This will be very important for the control design and testing.

## 6.7. Conclusion

Different scaling ideas were explored. Scaling the derivatives, their uncertainty, and scaling the gain of the model. Scaling the parameters may have the opposite effect, thus, it cannot be used. Scaling the uncertainty of the parameters has a more positive effect since it enlarges the uncertainty region, this is a conservative way to solve the problem, and it may not work if the eigenvalues are located in a larger region, however, the controller tuned for the larger uncertainty will be more robust and less sensitive to the true model. Finally, it is concluded that a gain scaling must be present, the models have different magnitudes which will reflect on the control gains and stability margins, thus, scaling the gains is a must.

In the next chapter, the models will be scaled through parameters uncertainty and gains only, the parameters will not be scaled explicitly. Then, an $H_\infty$-based robust controller will be designed for each scaled model and applied to the true model to assess the validity of the approach through several metrics such as gain and phase margins, the variance accounted for (VAF) of the roll angle tracking, and settling time and overshoot of an applied step response.

# 7 | $H_\infty$ controller

When any vehicle's dynamics are identified, the identified model usually consists of parameters that are defined by a probability density function, usually a Gaussian density expressed in terms of an expected value and a standard deviation.

It is important to design a controller such that the sensitivity to the parameters is attenuated and the required performance is achieved.

This can be achieved by designing a Robust Controller, that guarantees stability and if possible performance while keeping the control effort low. The Robust Controller will design using the $H_\infty$ synthesis, which is an optimization method that minimizes the norm of the plant while respecting the constraints.

## 7.1. $H_\infty$ Synthesis

The model is defined as a feedback loop with three weights $W_1(s)$, $W_2(s)$, and $W_3(s)$ that define the stability, control effort, and performance, respectively. The $H_\infty$ norm is defined as,

$$H_\infty = \left\| \begin{matrix} W_1(s)S(s) \\ W_2(s)Q(s) \\ W_3(s)F(s) \end{matrix} \right\|_\infty < 1 \tag{7.1}$$

where, $S(s)$ is the sensitivity function, $Q(s)$ is the control sensitivity function and $F(s)$ is the complementary sensitivity function. The block diagram is shown in Figure 7.1

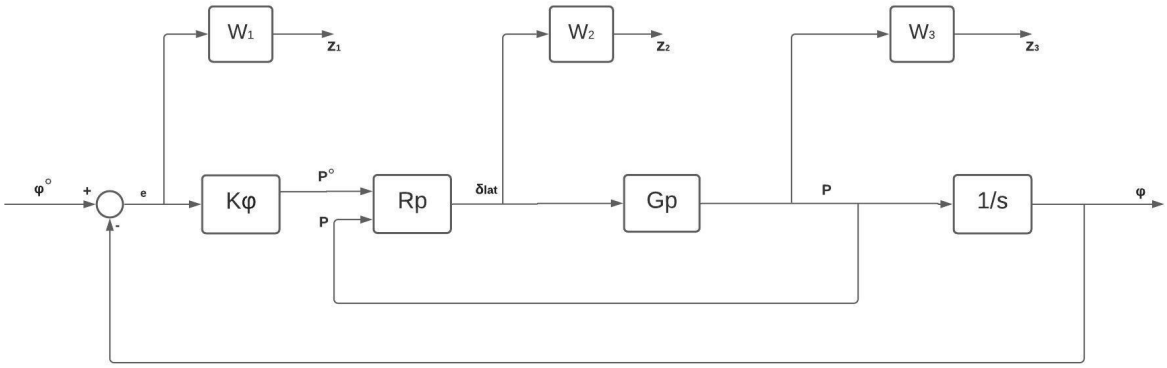


Figure 7.1: $H_\infty$ loop.

The $H_\infty$ controller consists of two blocks, a 2-dof PID control block ($R_p$), and a gain ($K_\phi$). The PID block has mainly 3 tunable parameters, $K_p$, $K_i$, and $K_d$, which will be tuned using the $H_\infty$ optimization algorithm.

The requirements for the performance of the closed-loop system are given below,

1. $\omega_n > 10$ rad/s, settling time $< 0.5$s
2. $\xi < 0.9$, Percentage overshoot $< 0.15\%$
3. Maximum peak, $M \simeq 1.3$
4. No control effort limitation.

All the models will be scaled with respect to the target multirotor through the parameters uncertainty and gain using the Hub-to-Hub distance, and the Robust Controller tuned based on the scaled models will be applied to the true model to see if the stability and performance requirements will be respected.

500 samples will be generated from the uncertain plants, with the uncertainty of $\pm 3\sigma$, then a simulation is done for two signals, a step input and input signal (Figure 7.2). Monte Carlo[3] approach is used to analyze the performance of the controllers. For the Step input, the Overshoot and Settling Time will be used to assess the performance., for the input signal the variance accounted for (VAF) to assess how well the controller can track the input set-point, while the phase and gain margins will be used to assess the handling qualities and stability of the system.

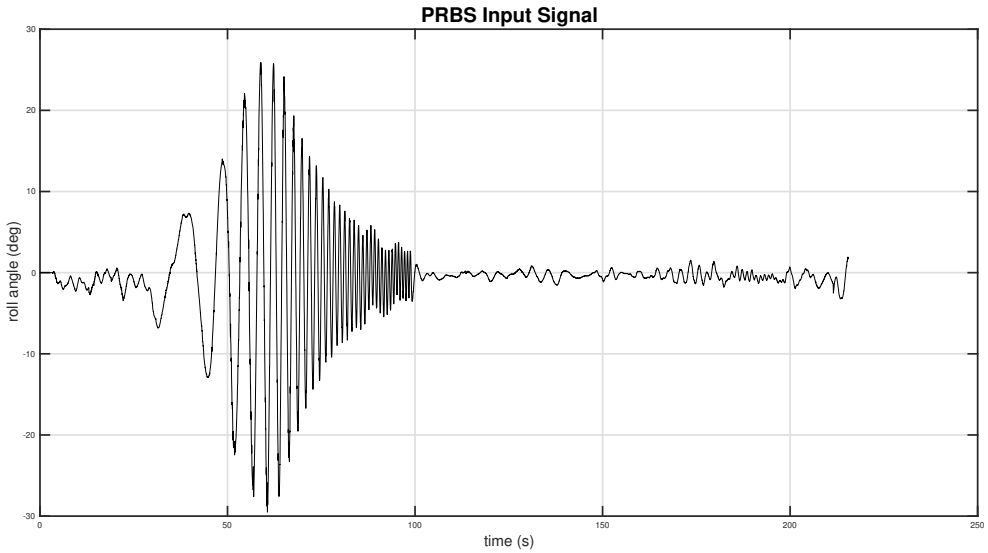


Figure 7.2: Input signal.

### 7.1.1. ANT-R as Target

In this section, the multirotors will be scaled according to the ANT-R, and a controller will be designed for each model, then all the different controllers will be applied to the true ANT-R model. Then, the performance, i.e. handling qualities will be evaluated.

Table-7.1 shows the gains of the controllers designed based on each scaled model and the true model.

| | **ANT-R** (true) | **ANT-X** (scaled) | **CARRIER-1** (scaled) | **ADAM-0** (scaled) |
|---|---|---|---|---|
| $K_p$ | 0.201 | 0.583 | 0.507 | 0.386 |
| $K_i$ | 9.17 | 19.5 | 9.45 | 3.76 |
| $K_d$ | $2.09e{-}07$ | $6.85e{-}06$ | $4.39e{-}07$ | $4.64e{-}05$ |
| $K_\phi$ | 11.98 | 11.93 | 9.409 | 13.69 |

Table 7.1: $H_\infty$ control gains based on ANT-R as target.

The following figures show the performance of the controller optimized using the true ANT-R model and applied to the true ANT-R model. The gain margin in this case is infinite.

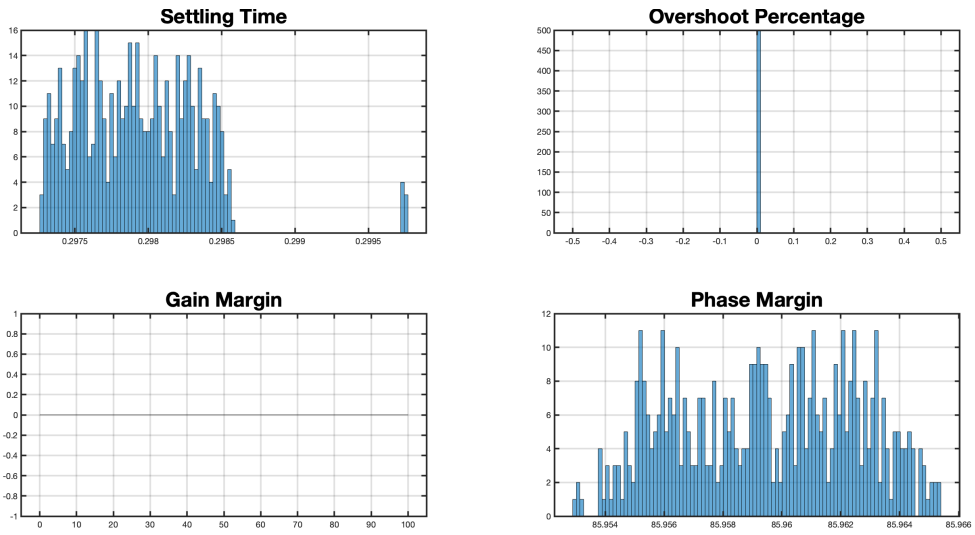


Figure 7.3: ANT-R performance and stability using ANT-R based controller.

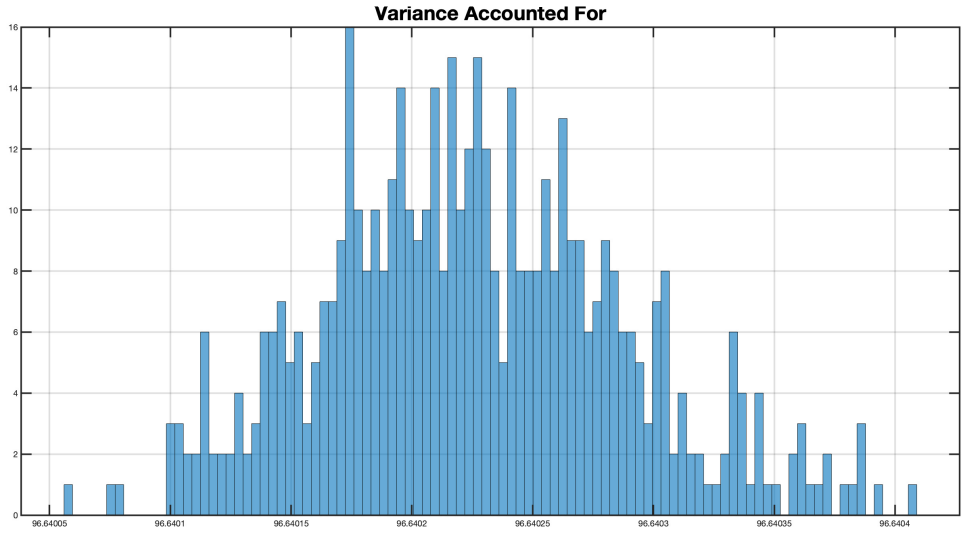


Figure 7.4: ANT-R VAF using ANT-R based controller.

The following figures show the performance of the controller optimized using the scaled ANT-X model and applied to the true ANT-R model. The gain margin is infinite for all samples.

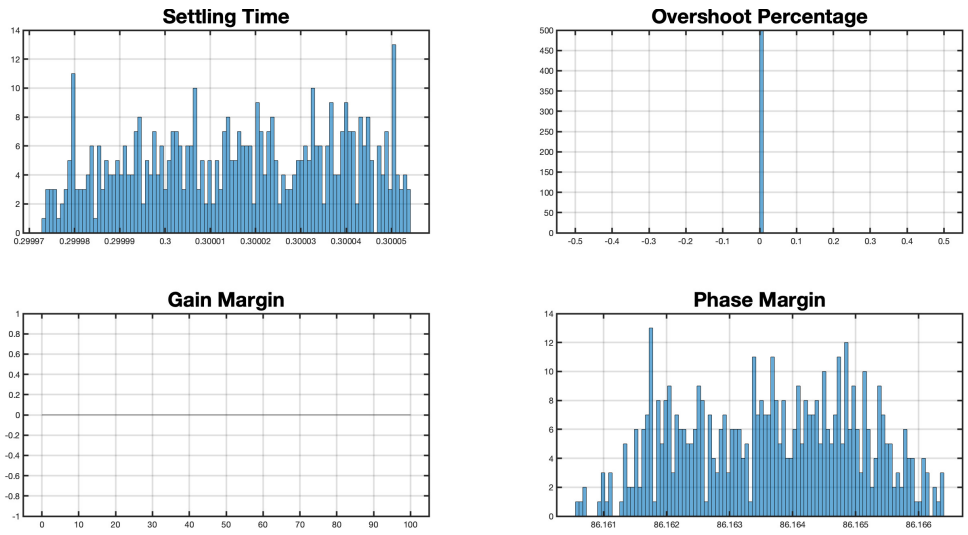


Figure 7.5: ANT-R performance and stability using ANT-X based controller.

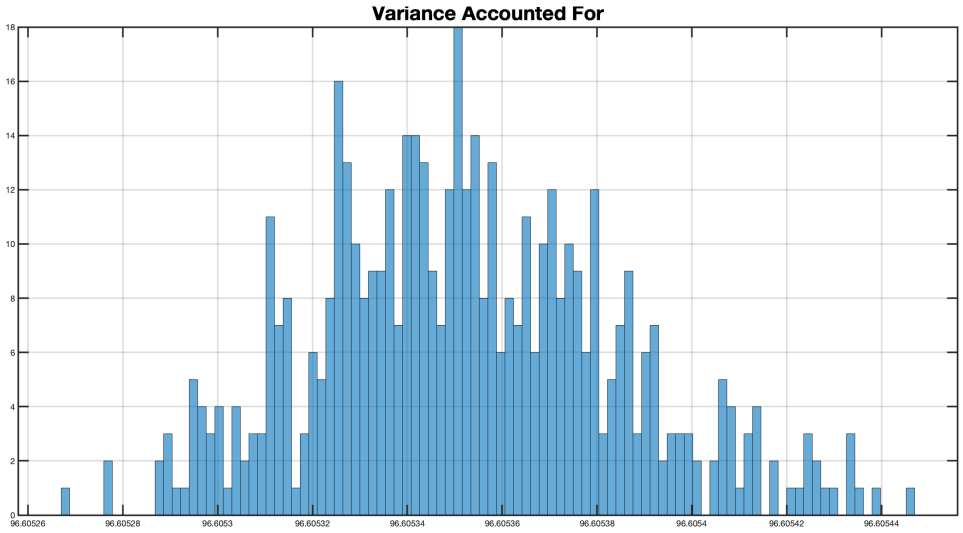


Figure 7.6: ANT-R VAF using ANT-X based controller.

While the following figures show the performance of the controller optimized using the scaled ADAM-0 model and applied to the true ANT-R model.

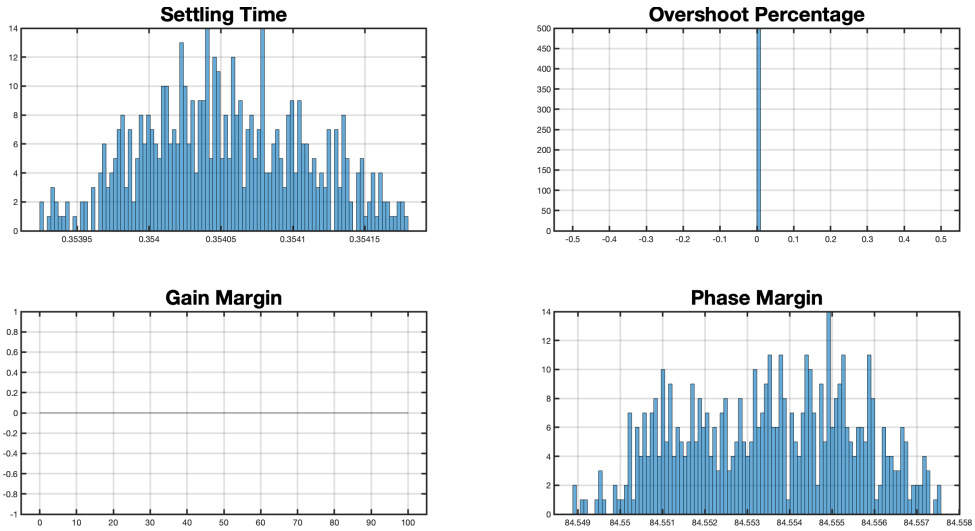


Figure 7.7: ANT-R performance and stability using ADAM-0 based controller.

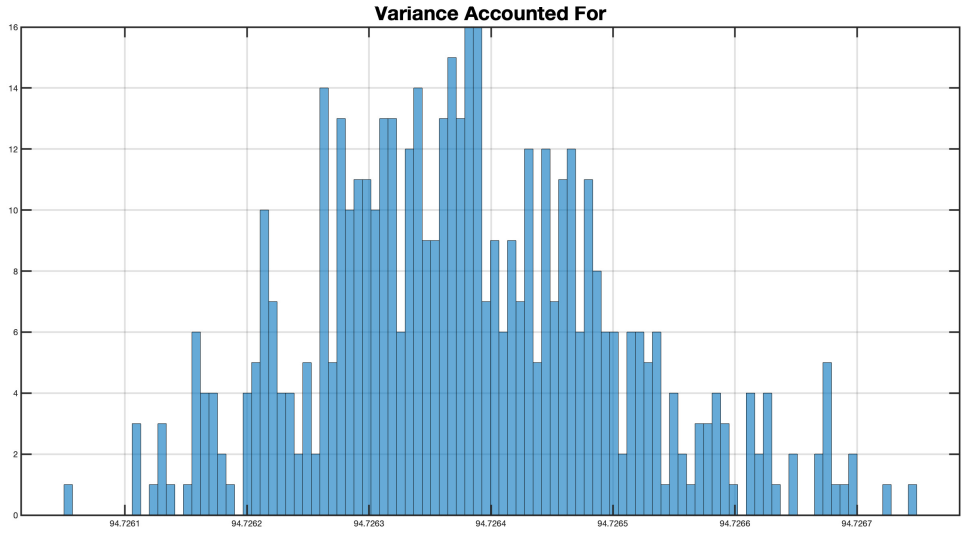


Figure 7.8: ANT-R VAF using ADAM-0 based controller.

While the following figures show the performance of the controller optimized using the scaled CARR-1 model and applied to the true ANT-R model. The gain margin is infinite for all samples.

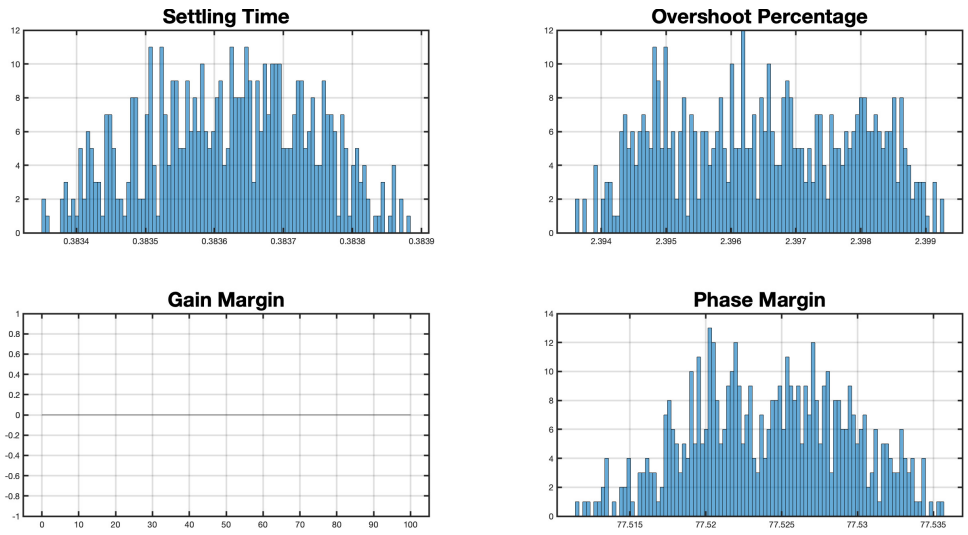


Figure 7.9: ANT-R performance and stability using CARR-1 based controller.

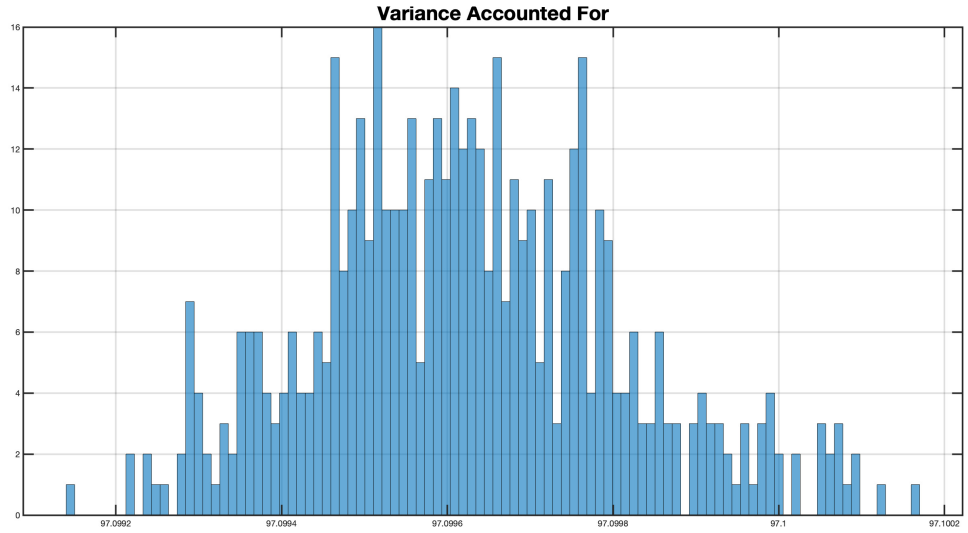


Figure 7.10: ANT-R VAF using CARR-1 based controller.

The results show that all controller track the input very well (high VAF), while respecting the settling time requirement, and have good phase and gain margins, however, the CARRIER-1 based controller causes 2% overshoot which is higher than the requirement (0.15%). It is still a good result given the roll angle was accurately tracked. Figure 7.11 shows the control input to the model.

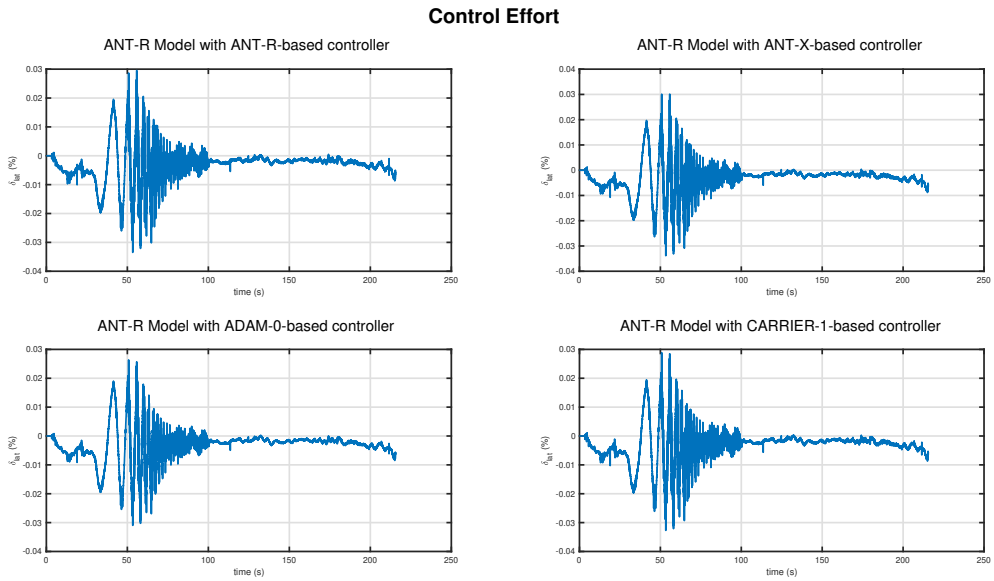


Figure 7.11: ANT-R control effort $\delta_{lat}$.

### 7.1.2. ANT-X as Target

In this section, the multirotors will be scaled with respect to the ANT-X, and a controller will be designed for each model, then all the different controllers will be applied to the true ANT-X model. Finally, the performance, i.e. handling qualities will be evaluated.

Table-7.2 shows the gains of the controllers designed based on each scaled model and the true model.

| | **ANT-R** (scaled) | **ANT-X** (true) | **CARRIER-1** (scaled) | **ADAM-0** (scaled) |
|---|---|---|---|---|
| $K_p$ | 0.123 | 0.6 | 0.341 | 0.225 |
| $K_i$ | 3.2 | 35.8 | 2.21 | 0.987 |
| $K_d$ | $4.99e{-}07$ | $3.57e{-}06$ | $1.64e{-}05$ | $3.89e{-}04$ |
| $K_\phi$ | 11.81 | 12.04 | 12.49 | 6.258 |

Table 7.2: $H_\infty$ control gains based on ANT-X as target.

The following figures show the performance of the controller optimized using the scaled ANT-R model and applied to the true ANT-X model. The gain margin is infinite for all samples.

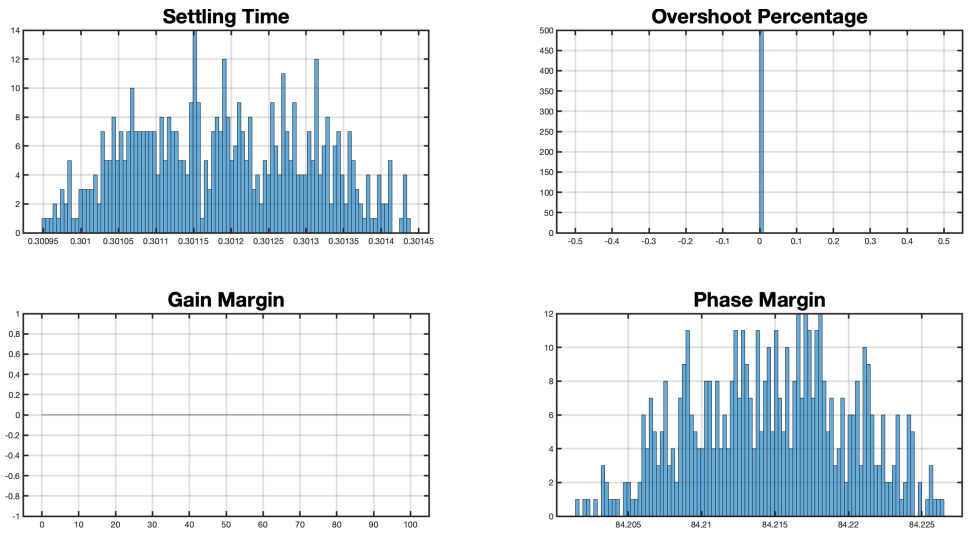


Figure 7.12: ANT-X performance and stability using ANT-R based controller.

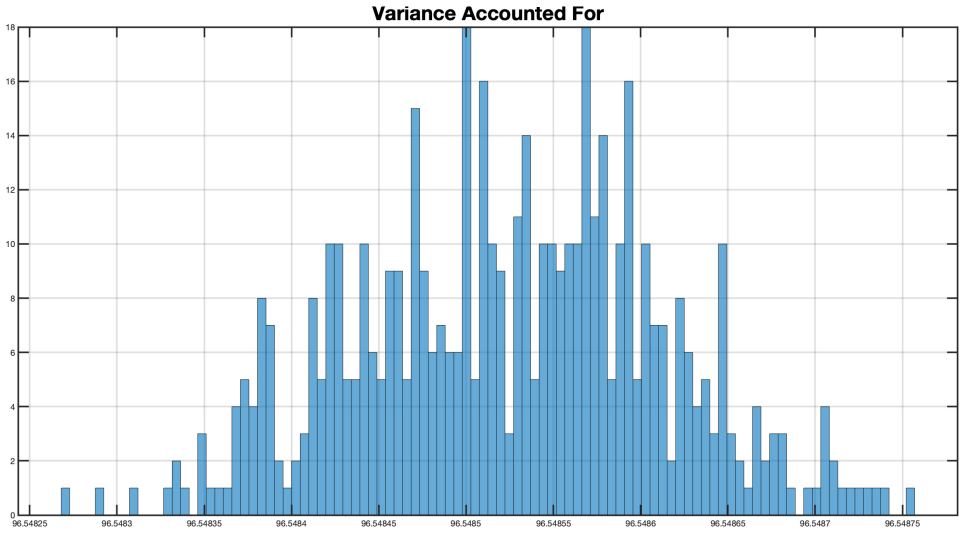


Figure 7.13: ANT-X VAF using ANT-R based controller.

The following figures show the performance of the controller optimized using the true ANT-X model and applied to the true ANT-X model. The gain margin is infinite for all samples.

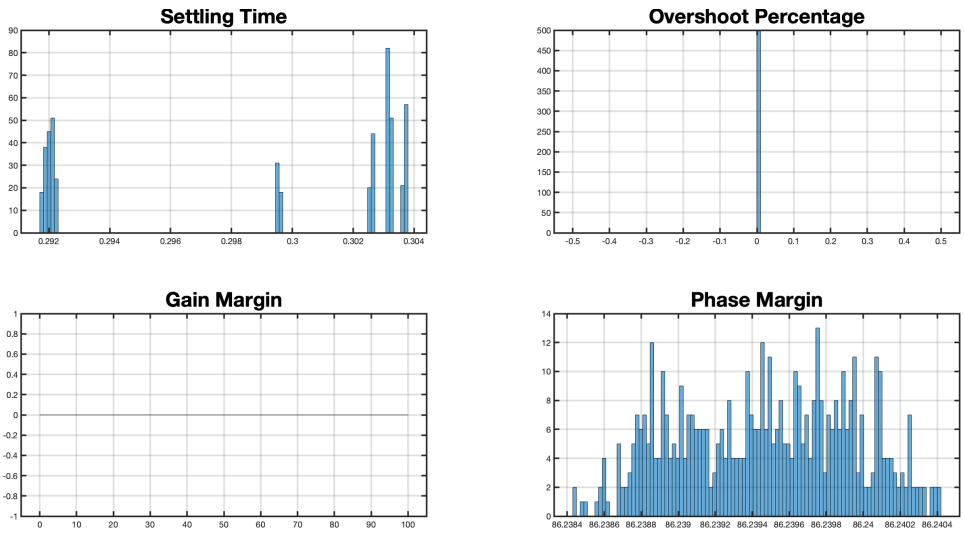


Figure 7.14: ANT-X performance and stability using ANT-X based controller.

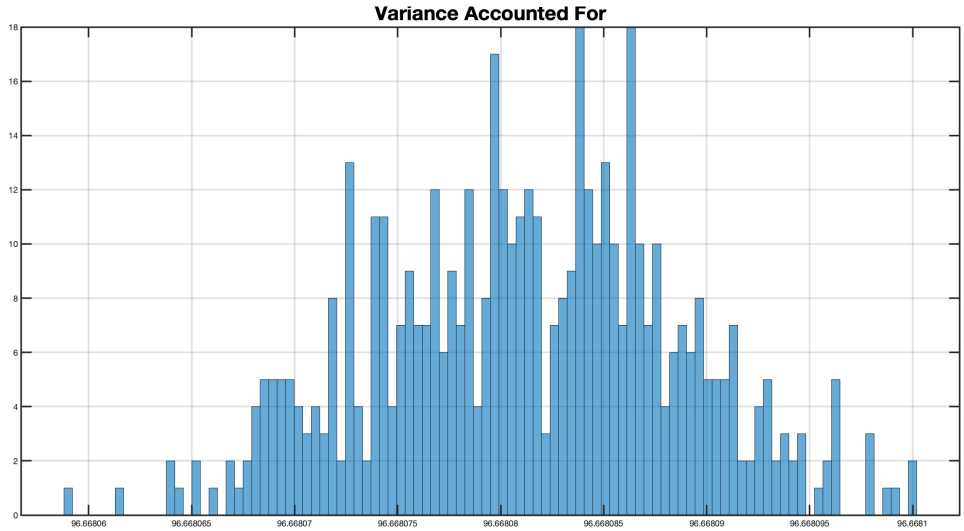


Figure 7.15: ANT-X VAF using ANT-X based controller.

While the following figures show the performance of the controller optimized using the scaled ADAM-0 model and applied to the true ANT-X model. The gain margin is infinite for all samples.

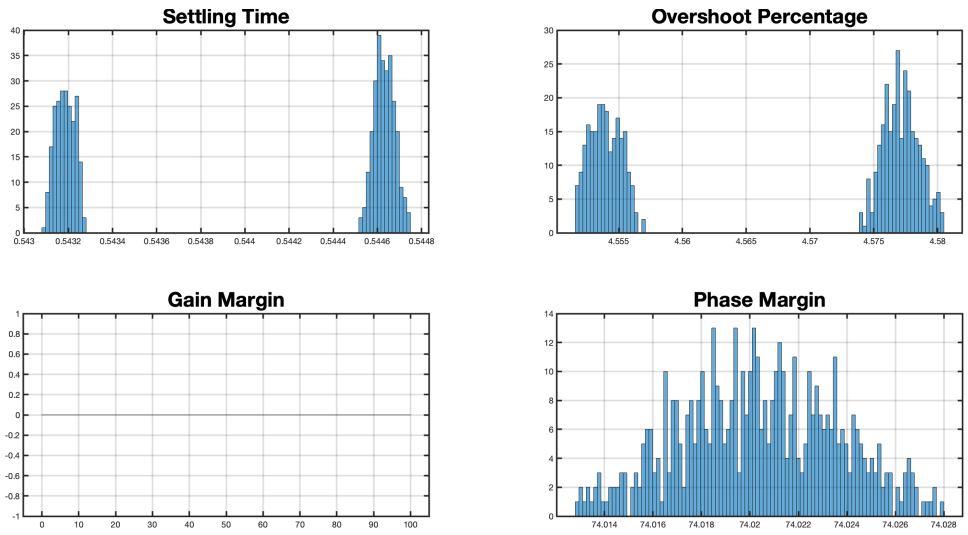


Figure 7.16: ANT-X performance and stability using ADAM-0 based controller.

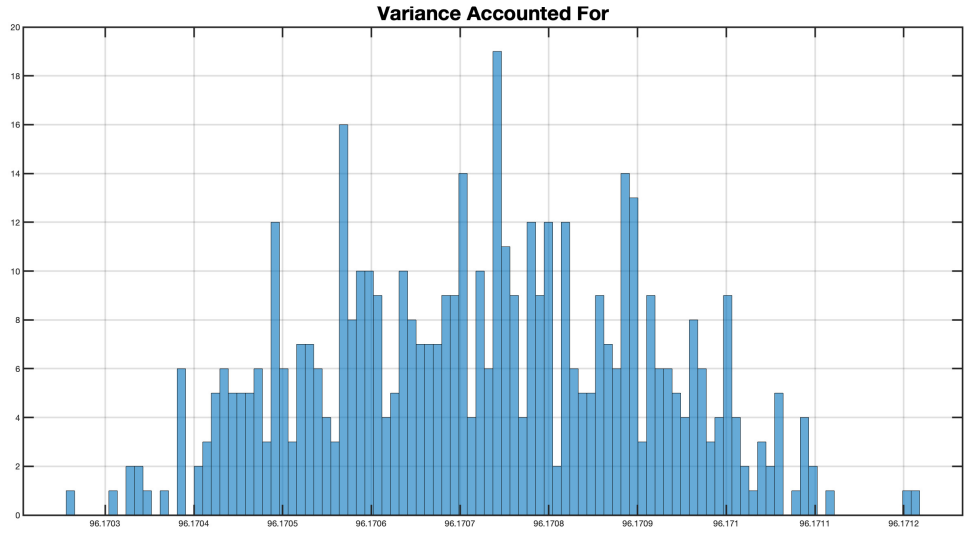


Figure 7.17: ANT-X VAF using ADAM-0 based controller.

While the following figures show the performance of the controller optimized using the scaled CARR-1 model and applied to the true ANT-X model. The gain margin is infinite for all samples.

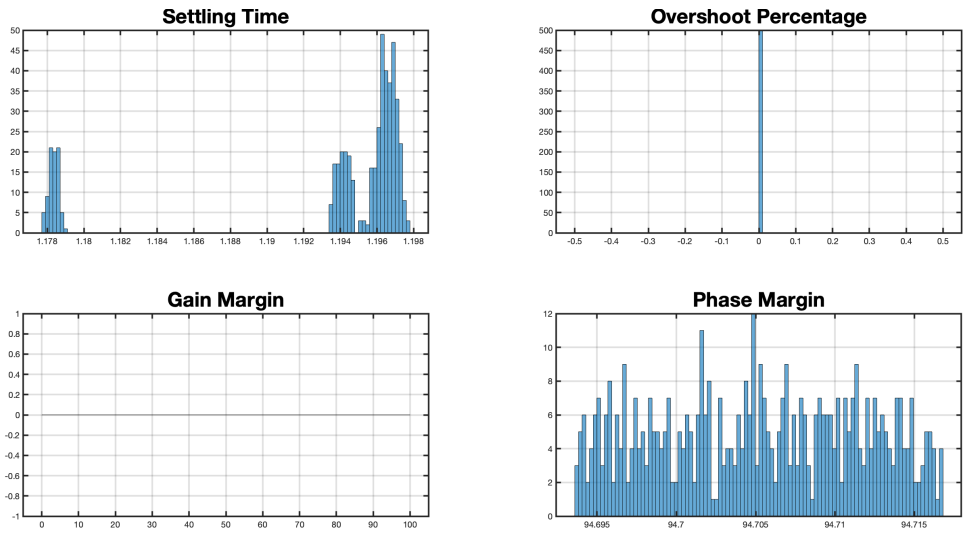


Figure 7.18: ANT-X performance and stability using CARR-1 based controller.

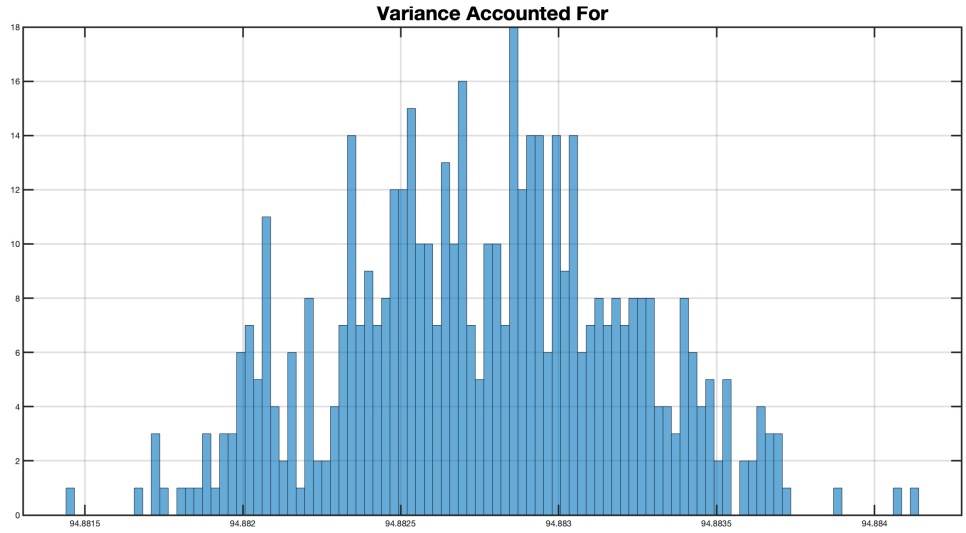


Figure 7.19: ANT-X VAF using CARR-1 based controller.

The results show that all controllers track the set-point accurately, while respecting the setting time requirement, and have good phase and gain margins, however, the CARRIER-1 based controller causes >4% overshoot which is higher than the requirement (0.15%). It is still a good result given the roll angle was accurately tracked. Figure 7.20 shows the control input to the model.

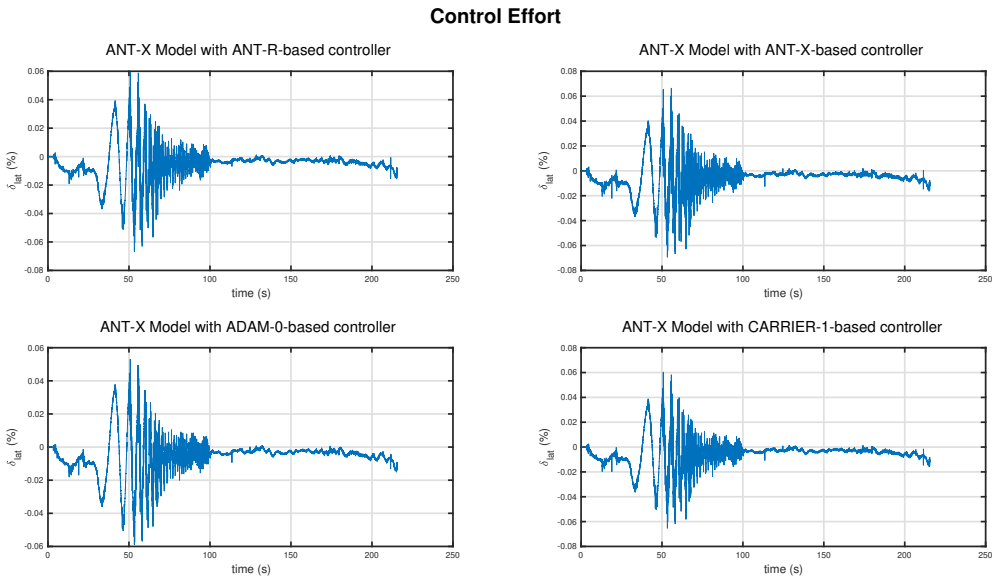


Figure 7.20: ANT-X control effort $\delta_{lat}$.

### 7.1.3. ADAM-0 as Target

In this section, the multirotors will be scaled with respect to the ADAM-0, and a controller will be designed for each model, then all the different controllers will be applied to the true ADAM-0 models. Finally, the performance, i.e. handling qualities will be evaluated.

Table-7.3 shows the gains of the controllers designed based on each scaled model and the true model.

| | **ANT-R** (scaled) | **ANT-X** (scaled) | **CARRIER-1** (scaled) | **ADAM-0** (true) |
|---|---|---|---|---|
| $K_p$ | 0.213 | 0.604 | 0.645 | 1.07 |
| $K_i$ | 5.13 | 3.09 | 6.97 | 47.1 |
| $K_d$ | $1.39e{-}06$ | $1.44e{-}05$ | $8.17e{-}06$ | $4.43e{-}05$ |
| $K_\phi$ | 11.54 | 13.88 | 11.37 | 10.68 |

Table 7.3: $H_\infty$ control gains based on ANT-X as target.

The following figures show the performance of the controller optimized using the scaled ANT-R model and applied to the true ADAM-0 model. The gain margin is infinite for all samples.

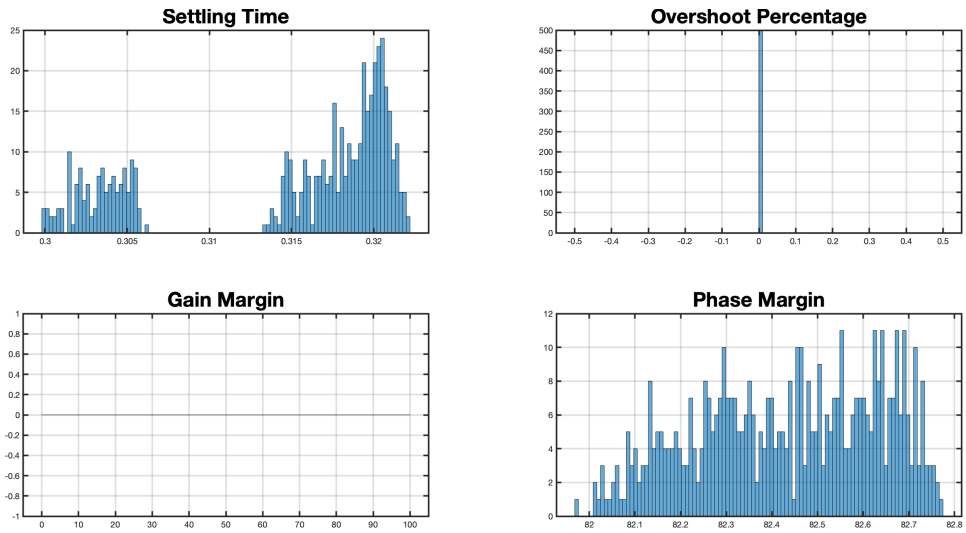


Figure 7.21: ADAM-0 performance and stability using ANT-R based controller.

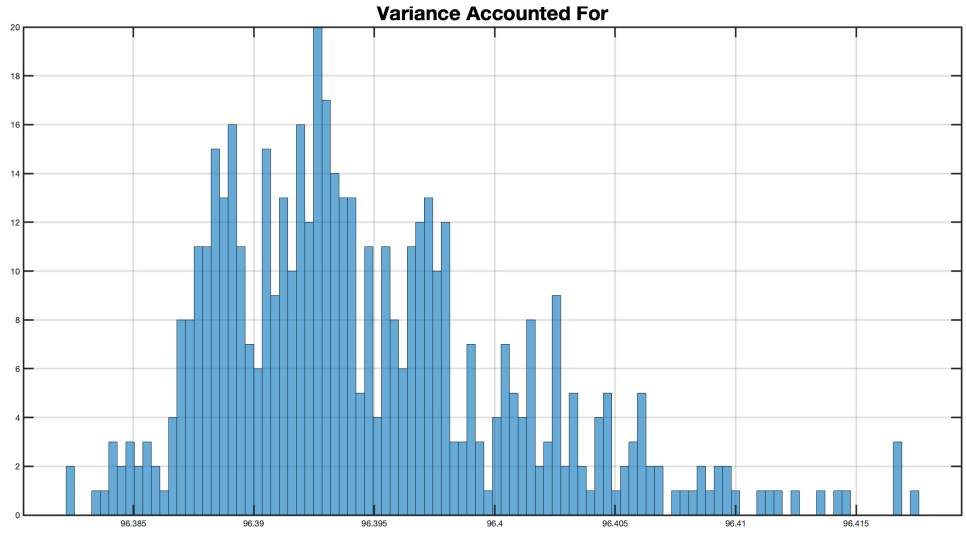


Figure 7.22: ADAM-0 VAF using ANT-R based controller.

The following figures show the performance of the controller optimized using the scaled ANT-X model and applied to the true ADAM-0 model. The gain margin is infinite for all samples.

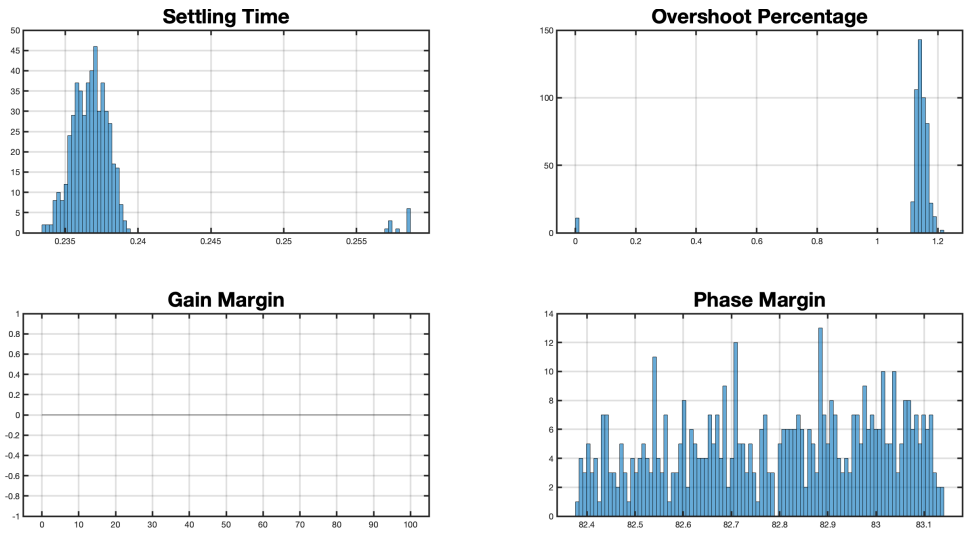


Figure 7.23: ADAM-0 performance and stability using ANT-X based controller.

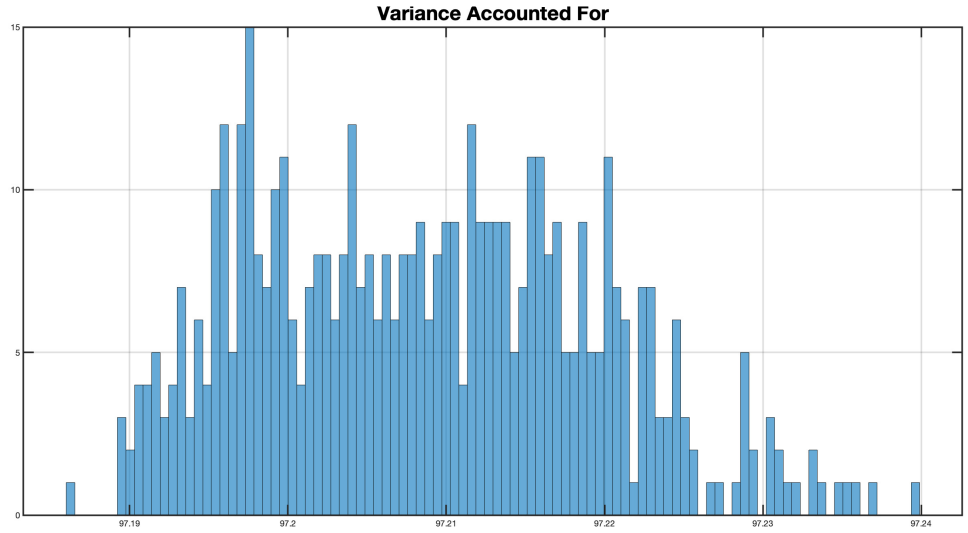


Figure 7.24: ADAM-0 VAF using ANT-X based controller.

While the following figures show the performance of the controller optimized using the true ADAM-0 model and applied to the true ADAM-0 model. The gain margin is infinite for all samples.

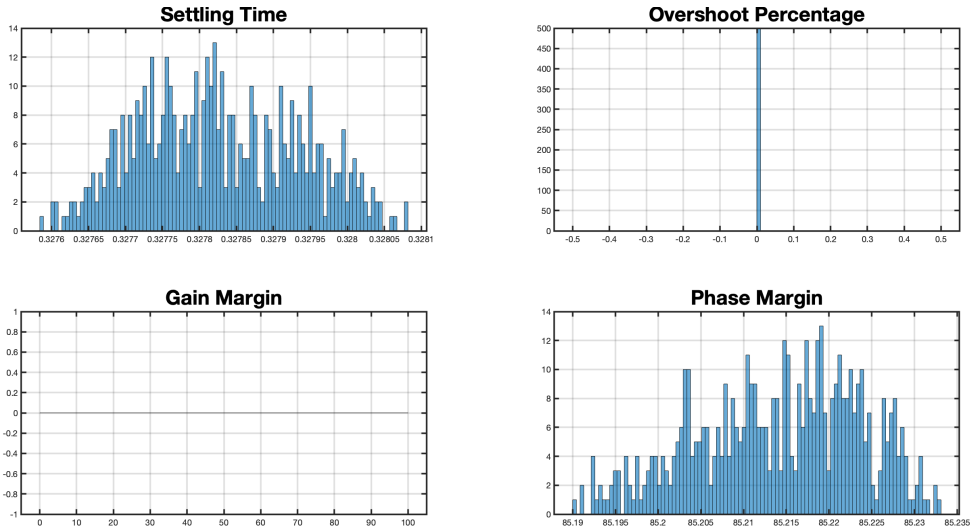


Figure 7.25: ADAM-0 performance and stability using ADAM-0 based controller.

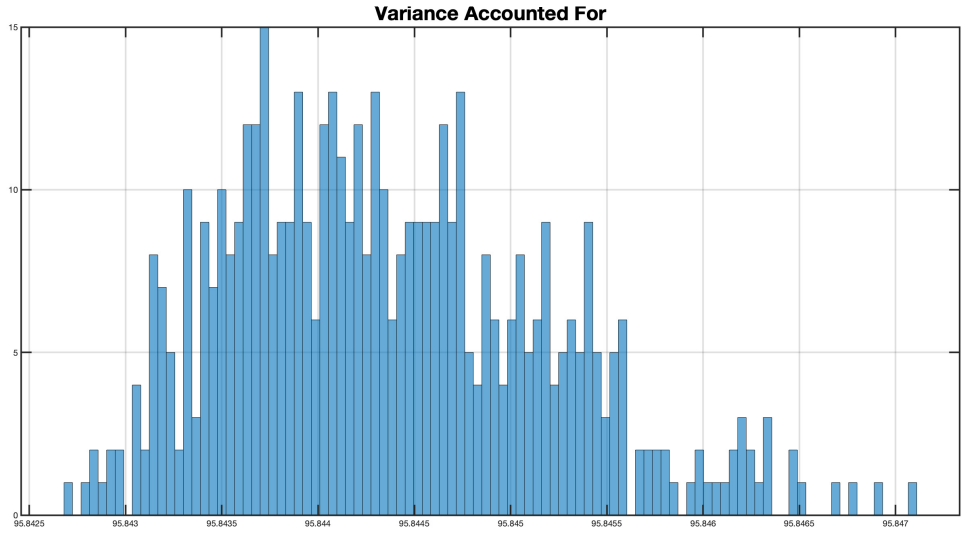


Figure 7.26: ADAM-0 VAF using ADAM-0 based controller.

While the following figures show the performance of the controller optimized using the scaled CARR-1 model and applied to the true ADAM-0 model. The gain margin is infinite for all samples.

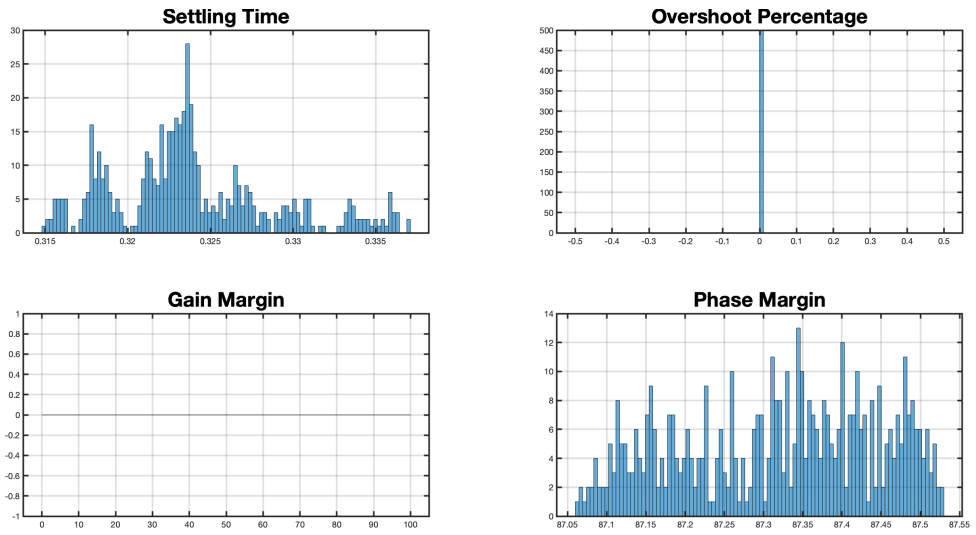


Figure 7.27: ADAM-0 performance and stability using CARR-1 based controller.

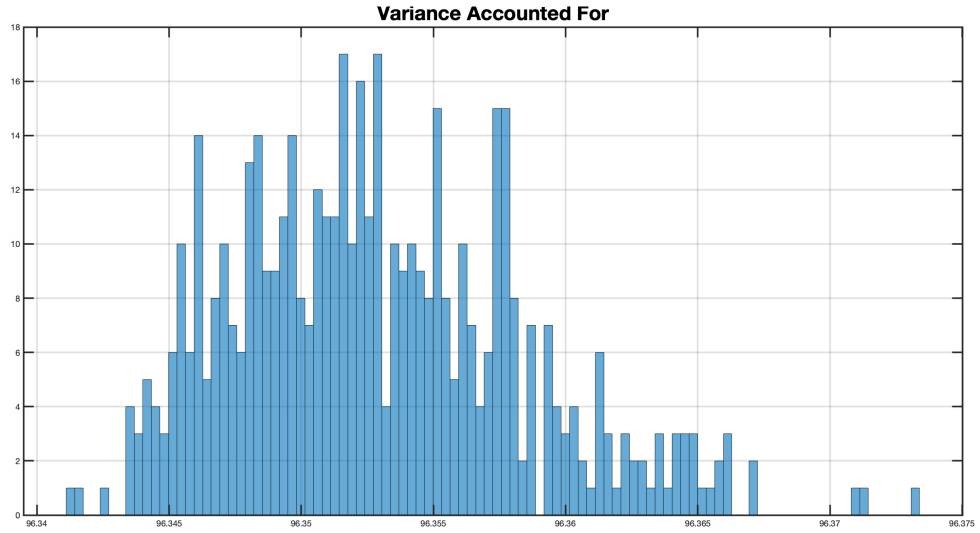


Figure 7.28: ADAM-0 VAF using CARR-1 based controller.

The results show that all controllers track the set-point accurately, respect the setting time requirement, and have good phase and gain margins, however, the ANT-X based controller causes >1% overshoot which is higher than the requirement (0.15%). It is still a good result given the roll angle was accurately tracked. Figure 7.29 shows the control input to the model.

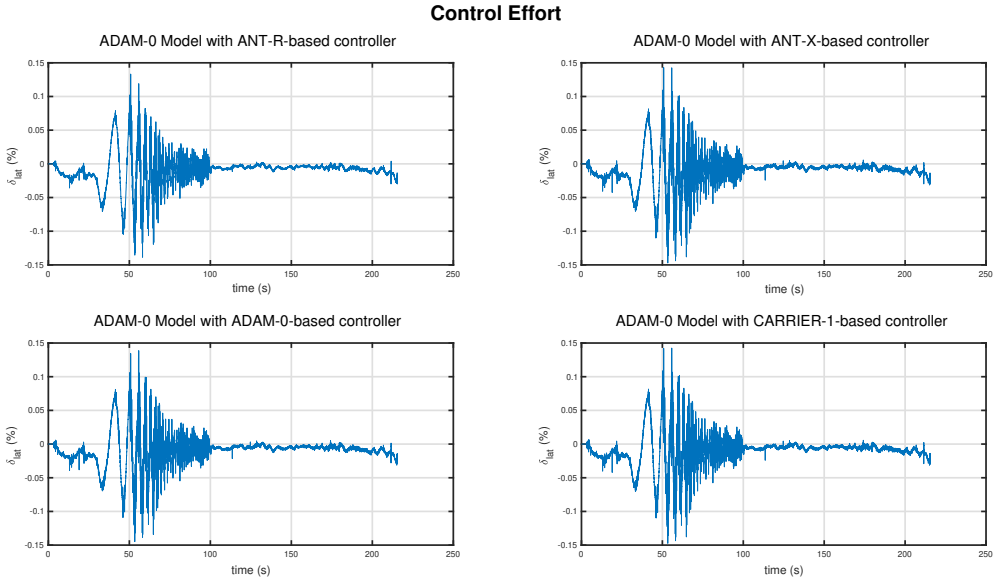


Figure 7.29: ADAM-0 control effort $\delta_{lat}$.

### 7.1.4. CARRIER-1 as Target

In this section, the multirotors will be scaled with respect to the CARRIER-1, and a controller will be designed for each model, then all the different controllers will be applied to the true CARRIER-1 model. Finally, the performance, i.e. handling qualities will be evaluated.

Table-7.3 shows the gains of the controllers designed based on each scaled model and the true model. Notice that since the Froude Number of CARRIER-1 and ADAM-0 is unity, the optimal gains are identical to the ones obtained in the previous section. However, the model they will be applied to will be different.

The following figures show the performance of the controller optimized using the scaled ANT-R model and applied to the true CARRIER-1 model. The gain margin is infinite for all samples.

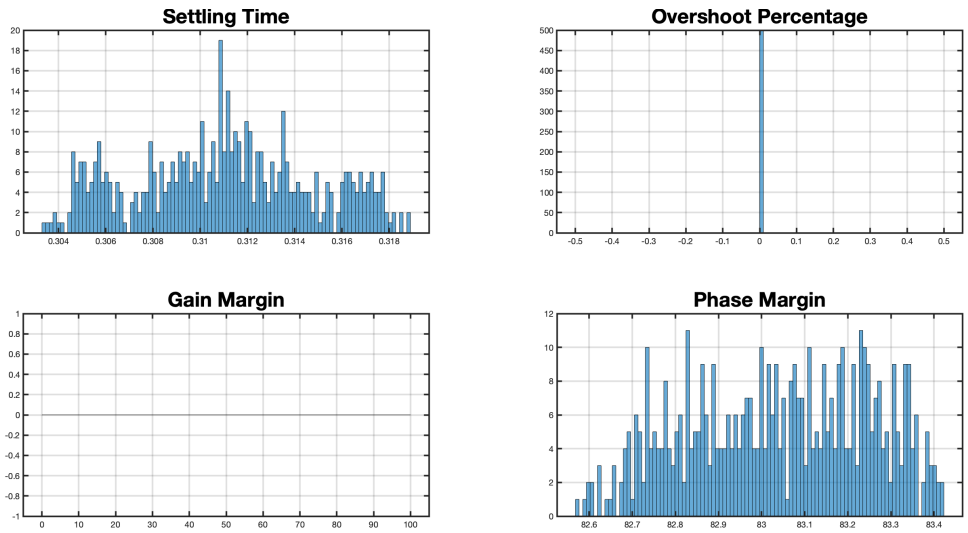


Figure 7.30: CARRIER-1 performance and stability using ANT-R based controller.

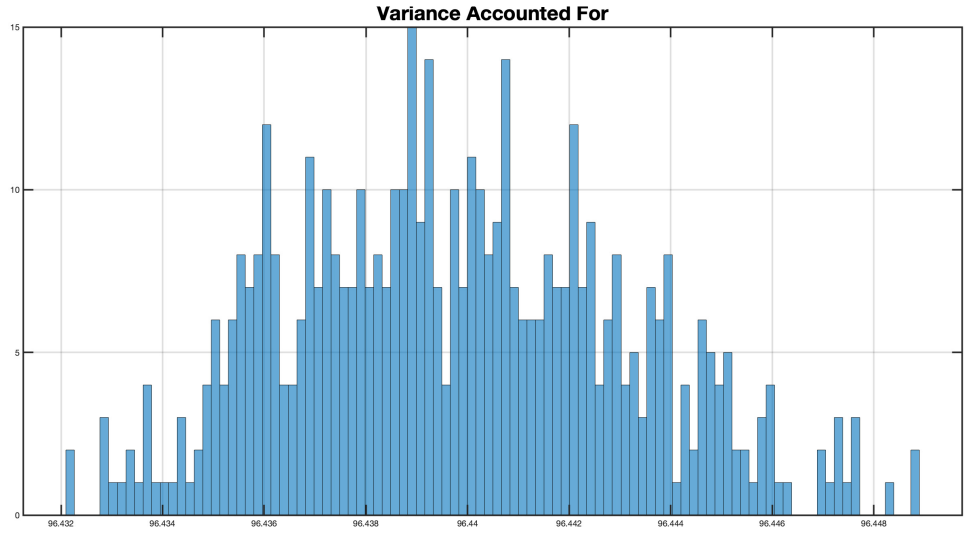


Figure 7.31: CARRIER-1 VAF using ANT-R based controller.

The following figures show the performance of the controller optimized using the scaled ANT-X model and applied to the true CARRIER-1 model. The gain margin is infinite for all samples.

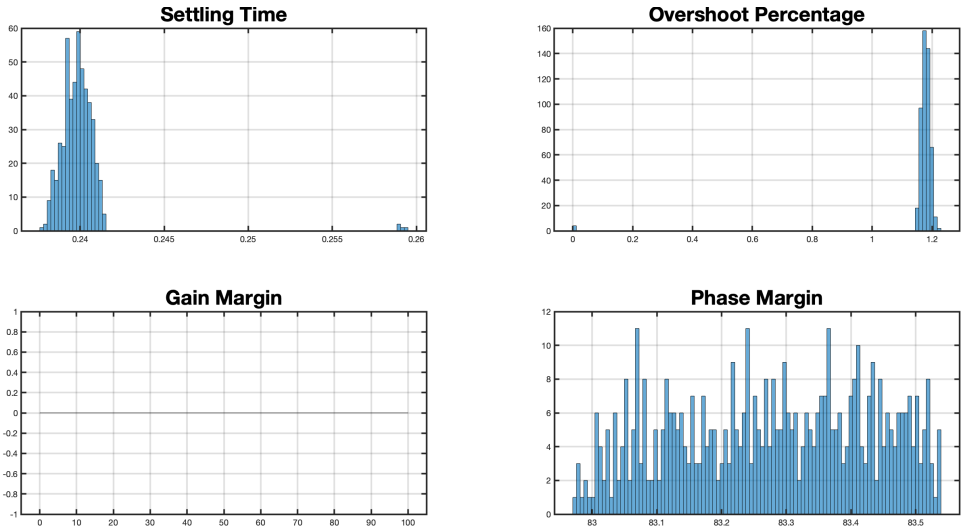


Figure 7.32: CARRIER-1 performance and stability using ANT-X based controller.

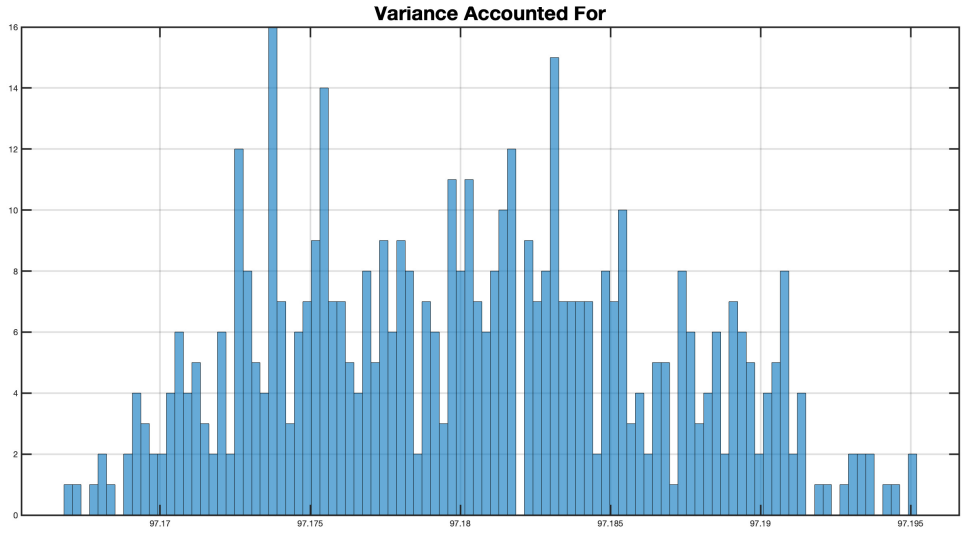


Figure 7.33: CARRIER-1 VAF using ANT-X based controller.

While the following figures show the performance of the controller optimized using the scaled ADAM-0 model and applied to the true CARRIER-1 model. The gain margin is infinite for all samples.

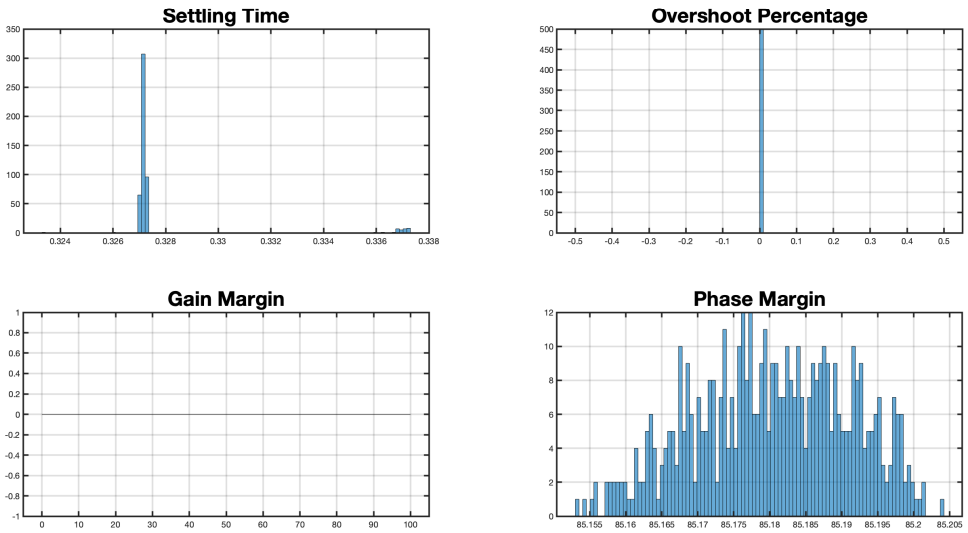


Figure 7.34: CARRIER-1 performance and stability using ADAM-0 based controller.

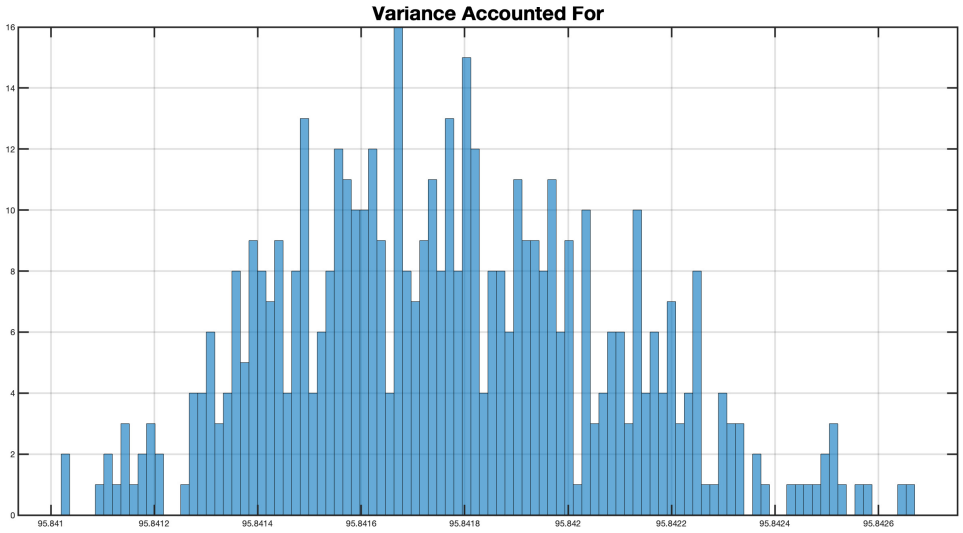


Figure 7.35: CARRIER-1 VAF using ADAM-0 based controller.

While the following figures show the performance of the controller optimized using the true CARRIER-1 model and applied to the true CARRIER-1 model. The gain margin is infinite for all samples.

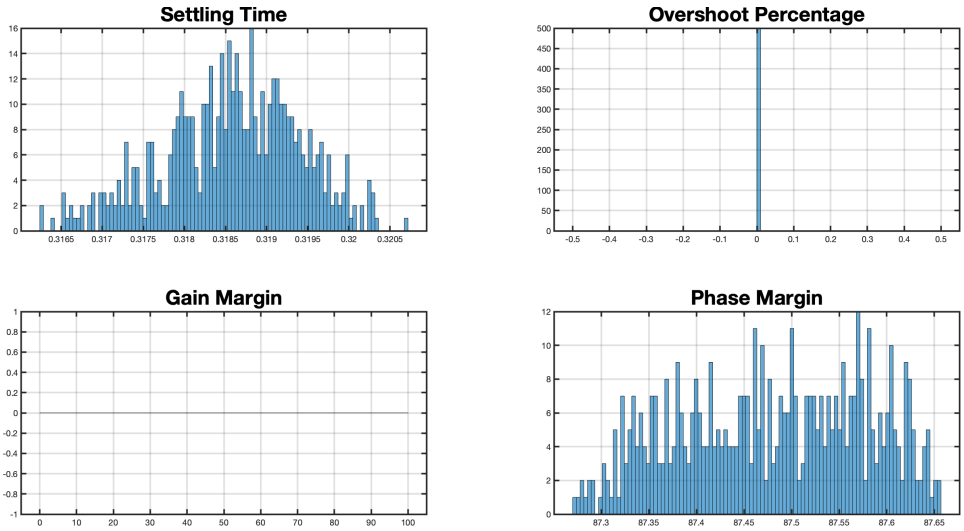


Figure 7.36: CARRIER-1 performance and stability using CARR-1 based controller.

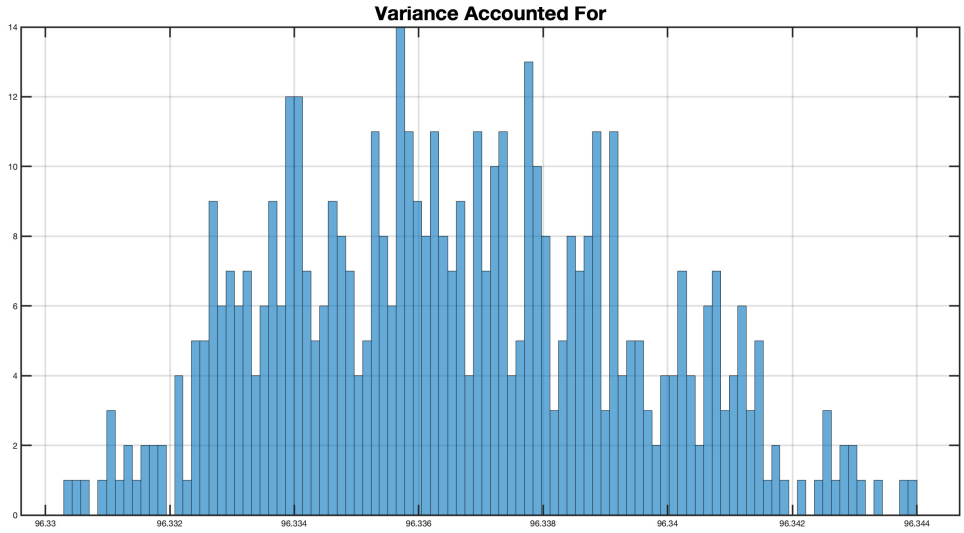


Figure 7.37: CARRIER-1 VAF using CARRIER-1 based controller.

The results show that all controllers track the set-point well, respect the setting time requirement, and have good phase and gain margins, however, the ANT-X based controller causes >1% overshoot which is higher than the requirement (0.15%). It is still a good result given the roll angle was accurately tracked. Figure 7.38 shows the control input to the model.

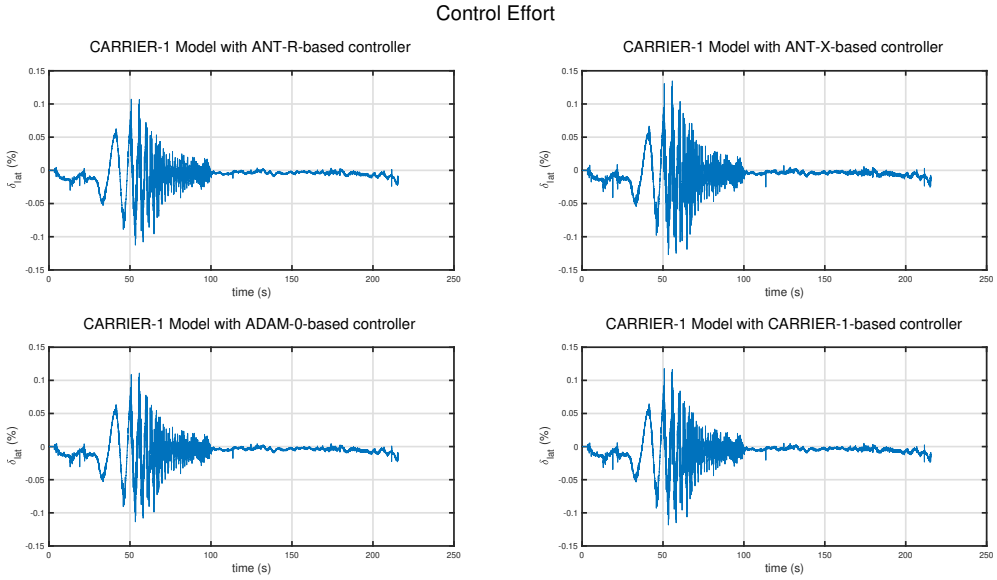


Figure 7.38: CARRIER-1 control effort $\delta_{lat}$.

## 7.2. Conclusion

Different controllers were optimized with respect to different, scaled and true, models then added to the models to close the inner loop, roll damping, and outer loop, which tracks the set-point input. All controllers performed well, some violate the performance requirements but overall, it is considered acceptable, even though the uncertainty was scaled up, and then a standard deviation of $3\sigma$ was used to test the models. This is to say that the multicopters are inherently similar, and one controller can provide decent performance and good stability.

The control effort is also not exhausted, the input is almost the same regardless of the controller. This is not surprising since the gains of the controllers are comparable for all scaled and true models, this is probably because the multicopters dynamics are already similar (see Table 3.1).

# 8 | Conclusion and future work

## 8.1. Conclusion

Froude scaling is a very appealing idea. Being able to get an approximate model for a rotorcraft without even running the motors is money- and time-saving. However, in engineering, if something is simple then it is probably wrong, **"Sometimes, simple is simply not enough, or worse is a way of faking comprehension when one does not really grasp mechanism nor seek understanding."**[7]

Reducing the rotorcraft to a number that depends on one factor is simply not correct, the results from [2] could have been a coincidence, where the rotorcrafts might have been already similar and the scaling was enough to close the gap.

The Froude Scaling technique might be a feasible technique, however, it needs to account for more than just the dimensions of the multirotor. The Hub-to-Hub distance was used in the analysis and the following conclusions can be drawn,

1. The Hub-to-Hub distance is not representative of the model scaling (does not give the right scale)
2. The Hub-to-Hub distance (or any positive scale) does not scale in the right direction in the case of ANT-X, and in general, thus, driving the model away from the true model.
3. The eigenvalues are already located close to each other, however, the scaling makes them spread further away.

However, there is a pattern, it could be merely a coincidence, but it is interesting and worth exploring. The four rotorcrafts can be divided into two groups according to the eigenvalues, ANT-R and ADAM-0, ANT-X and CARRIER-1, for some reason, the dynamics are very similar in each group, and it could be a starting point to look for similarities

parameters.

### 8.1.1. Group 1: ANT-R and ADAM-0

It is clear from Figure 8.1 that the ANT-R$^{1.1}$ and ADAM-0$^{1.4}$ quadrotors dynamics are similar, the roll mode, for example, is almost identical, while phugoid mode shows an error in both radial and angular direction, i.e., real and imaginary parts or natural frequency and damping ratio of the mode.

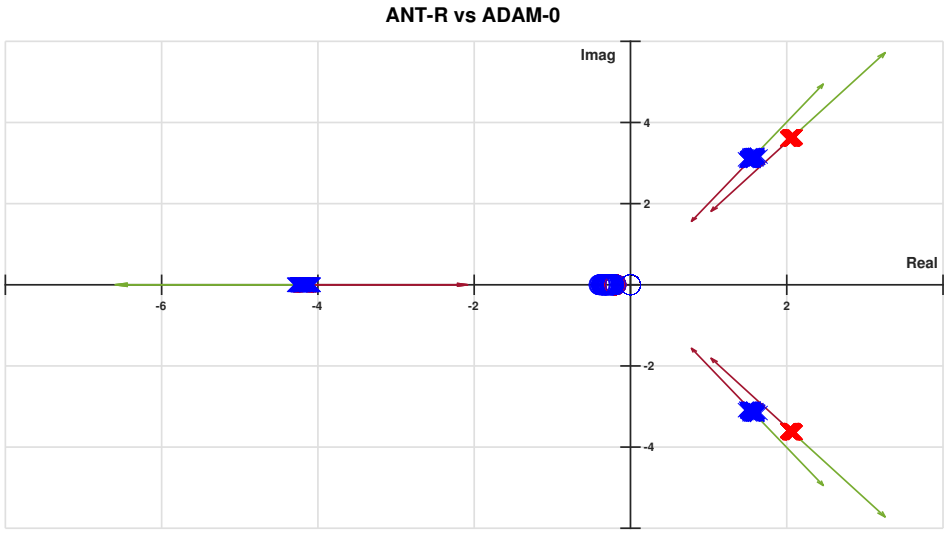


Figure 8.1: Comparing the dynamics of ANT-R (red) and ADAM-0 (blue) quadcopters.

While the eigenvalues are very similar, the magnitude accounts for most of the difference between the models, Figure 8.2 shows the ratio (scale) of the magnitudes of the ANT-R and ADAM-0 for various values of frequencies and the mean scale is also reported.

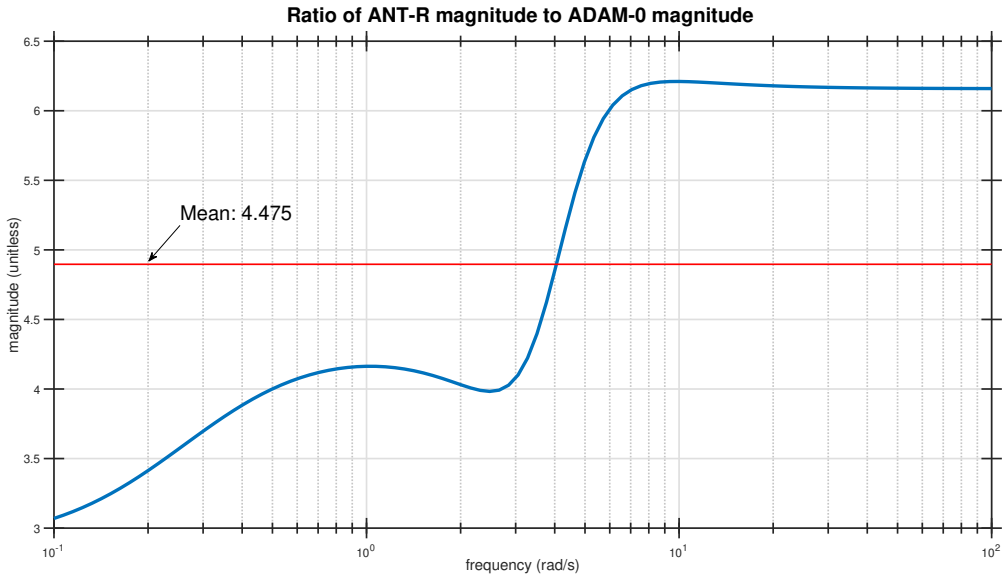


Figure 8.2: Ratio of ANT-R to ADAM-0 magnitude.

### 8.1.2. Group 2: ANT-X and CARRIER-1

It is clear from Figure 8.3 that the ANT-X[1.2] quadrotor and CARRIER-1[1.3] octarotor dynamics are similar, in fact, the roll incidence mode is almost identical, while the phugoid mode shows a very small error, i.e., real and imaginary parts or natural frequency and damping ratio of the mode are almost identical, refer to Table 3.1 for the values of the natural frequency and damping ratio.

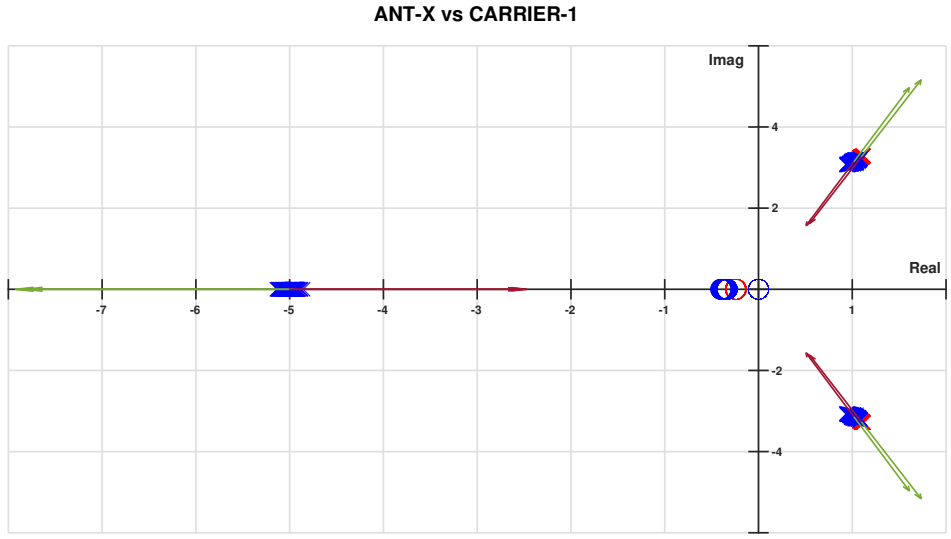


Figure 8.3: Comparing the dynamics of ANT-X quadcopter (red) and CARRIER-1 octacopter (blue).

It is evident that the ANT-X quadrotor and CARRIER-1 octarotor are very similar, even though they are very different in structure, with a different number of rotors, the heavier CARRIER-1 model's magnitude is about twice that of the lighter ANT-X model's (see Figure 8.4), this can be caused by various parameters and it would be insightful to explore what causes the difference, the number of rotors being the first probable parameter to cause such a difference.

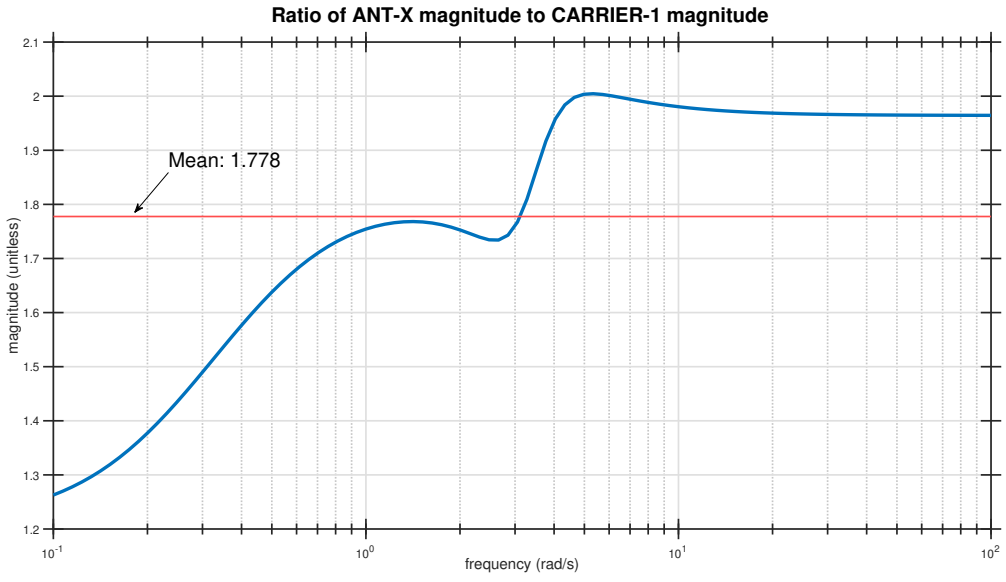


Figure 8.4: Ratio of ANT-X to CARRIER-1 magnitude.

## 8.2. Future Work

The scaling idea is still feasible, and from the analysis done, it is suggested to focus on at least two factors before thinking about scaling, rotor configuration, i.e., how the rotors are set up, and the number of rotors.

Also, in Chapter 7, closed-loop response using the optimized $H_\infty$ control is almost the same for the outer loop gain $K_\phi$, the proportion part $K_p$ and derivative part $K_d$ of the PID controller, while the integral part $K_i$ is different in some cases.

This could be caused by many reasons, however, it is useful to take the magnitude of the system into account when scaling, since the magnitude does not scale explicitly, but implicitly through the stability and control derivatives.

### 8.2.1. The Rotorcraft Configuration

In [6], the paper compares a quadcopter operating in multiple configurations, mainly, the plus and cross configurations, and identifies a model separately for each configuration.

The results are very insightful, which concludes that the rotor configuration does not by any means change the dynamics, in fact, the eigenvalues are not moving at all, however, the control authority is definitely not the same, where the pitch and roll control authority is up to about 30% greater for the cross-configuration since all four (as opposed to only two) rotors are used. This means that the gain given to the plus-configuration will be larger since only two rotors need to do the same job as four rotors in the cross-configuration.

This conclusion is very important and needs to be taken into account when scaling two multirotors with different configurations.

### 8.2.2. The Number of Rotors

Indeed, the number of rotors affects the maneuverability (control derivatives) and stability (stability derivatives) of the rotorcraft. The effect of the number of rotors is not readily available and needs to be understood before developing a scaling mechanism.

There is not a detailed study about how the number of rotors affects the dynamics, it is safe to assume the same about the configuration, which is that the control authority for a

hexacopter is higher than that of a quadcopter, but not the behavior of the eigenvalues, especially that the weight will be different and also affect the dynamics through inertia.

# Bibliography

[1] G. Fumai. Accuracy analysis of $PBSID_{opt}$-$H_\infty$ for multirotor uavs model identification. Master's thesis, Politecnico di Milano, Dec 2020.

[2] Ivler, Christina and Rowe, Elizabeth and Martin, James and Lopez, Mark and Tischler, Mark. System identification guidance for multirotor aircraft: Dynamic scaling and test techniques. *Journal of the American Helicopter Society*, 2021.

[3] Laura Ryan, Robert F. A monte carlo approach to the analysis of control system robustness. *Automatica*, 29:229–236, 1 1993.

[4] G. Lizza. Model identification and dynamic scaling for multirotor UAVs. Master's thesis, Politecnico di Milano, Apr 2021.

[5] Padovanews. The global multirotor drone market size is expected to reach $3.6 billion by 2028, rising at a market growth of 13.4% cagr during the forecast period, 9 2022.

[6] Robert J. Niemiec, F. Gandhi. A comparison between quadrotor flight configurations. *42nd European Rotorcraft Forum, Lille, France*, 2016.

[7] The Ethical Skeptic. When Simple is Just Simply Wrong, 3 2021. URL `https://theethicalskeptic.com/2018/05/27/when-simple-is-just-simply-wrong/`.